NORDA Technical Note 206

Naval Ocean Research and
Development Activity
NSTL, Mississippi 39529

Statistics of Vertical Shear from a Hemispheric Model

J. M. Harding
R. H. Preller
S. A. Piacsek

Ocean Science and Technology Laboratory
Numerical Modeling Division

September 1983

ABSTRACT

Using surface atmospheric momentum and heat fluxes derived from the Fleet Numerical Oceanography Center's weather prediction models, a computation of inertial and Ekman shear was done for the upper 400 m of the North Pacific and North Atlantic. Two 60-day periods were considered in November and December of 1976 and 1980. A capability to predict these types of shear in real-time, or near real-time, is demonstrated using the Navy's TOPS (Thermodynamic Ocean Prediction System) model. A statistical analysis of the vertical shear and associated Richardson number revealed that the time variability of shear appears to be linked primarily to the synoptic time scales of weather events; and the spatial distribution of shear instability ($0 \leq Ri \leq 0.25$) and high shear are closely related to the position of atmospheric fronts.

ACKNOWLEDGMENTS

The authors would like to extend their appreciation to Mr. Paul Martin for several useful discussions about the mixed-layer formulation within TOPS and to Ms. Mary Lou Morris for initial help with the computer code. Thanks are also due to Dr. Rudy Hollman for his patience with certain uncontrollable delays which interfered with the publication of this note.

Funding for this project was provided through the Ocean Measurements Programs of the NORDA Ocean Programs Management Office, under Program Element 63704N, Dr. Rudy Hollman program manager.

STATISTICS OF VERTICAL SHEAR FROM A HEMISPHERIC MODEL

1. Introduction

Gradients in the density and current velocity of the world's oceans strongly affect the propagation of internal waves. Such regions cause reflection, refraction, absorption and breaking of the waves. Under certain conditions, the internal waves can even grow in regions of velocity shear. To predict, in some deterministic and statistical sense, the spatial and temporal distribution of density and velocity gradients requires an extensive effort in ocean surveys and modeling.

Since temperature measurements are generally easier to carry out than current measurements, the available sets of temperature data are relatively abundant as compared to current data. High vertical resolution current measurements in the upper 400 meters (m) of the ocean are recent and relatively few, with only two or three measurements a year at selected locations. The maximum duration of continuous observations at any one site is about two weeks.

Both the results of field experiments (Evans (1982), Oakey (1982), Gregg and Sanford (1980), Gargett and Osborn (1981) and Gargett, et al. (1981)) and numerical simulations (Warn-Varnas and Dawson (1981), Martin (1982), Davis et al. (1981) have indicated that, in general, the largest shears in the ocean are associated with the inertial motions found just above, at, and just below the bottom of mixed layers. Exceptions to this rule can be found in regions of strong topographic effects, current instabilities and internal wave straining. The inertial motions are, in turn, generally strongly coupled to atmospheric weather events, and to a lesser extent to the generation of internal tides by the scattering of external tides off topographic features. The large spatial and temporal variability of atmospheric events implies that the extensive measurement survey needed to establish the relevant statistics of inertial shear in all parts of the world's oceans would be prohibitive, in terms of money and logistics. At the same time, the modeling efforts mentioned demonstrate that inertial and Ekman shears can be predicted rather successfully by mixed layer models using atmospheric forcing functions.

Thus, to obtain meaningful statistics on the seasonal and geographical variation of shear, along with its dependence on depth and synoptic weather conditions,

we decided to employ numerical models of the upper ocean. Besides yielding the desired statistics, the models might eventually enable us to make real time forecasts of shear 3-5 days in advance. The best candidate for such modeling is the TOPS (Thermodynamic Ocean Prediction System) model now operational at FNOC (Fleet Numerical Oceanography Center) (Clancy and Martin (1981); Clancy, et al. (1981 a, b)). This model uses the surface stress and heat flux values derived from the Navy's global weather prediction model NOGAPS (Naval Operational Global Atmospheric Prediction System) is initialized and updated by an analysis scheme that in turn uses the TOPS forecast products for first-guess fields, blending them with daily XBT observations and satellite-derived SST fields.

2. Brief Review of Observations and Modeling Efforts

Several investigators have used high resolution velocity and velocity/temperature microstructure profilers to measure the vertical distribution of shear, temperature, Richardson number and turbulence dissipation. Though their scientific objectives have varied, their cumulative efforts do give rise to a short time scale picture of vertical shear for limited areas of the world's oceans.

Gregg and Sanford (1980) made nearly simultaneous measurements of temperature and velocity gradients in three different geographical regions. Measurements in the Sargasso Sea indicated a concentration of shear in the 10-30 m depth range, near, and below the base of the mixed layer, with a peak value of 10^{-2} sec^{-1}.

Lange (1981) studied the nature of the small-scale velocity gradient fluctuations observed in the mixed layer during and after two storm events at the MILE (Mixed Layer Experiment) experimental site (50°N, 145°W). He found a strong correlation of wind-speed variations with velocity structures in a 20 m deep mixed layer. The rate of dissipation of mechanical energy was found to be as high as 5×10^{-2} $ergs\text{-}cm^{-3}\text{-}sec^{-1}$ during wind speeds of 20m/sec, and as low as 10^{-6} during light winds. A persistent vertical separation of temperature and velocity variance maxima at high wave numbers near the base of the mixed layer suggested that shear-induced entrainment continued for several days after the storm events subsided.

Gargett and Osborn (1981) studied the distribution of small-scale shear during the FAME (Fine and Microstructure Experiment) at three geographical sites. They

found that the dissipation had a clear dependence on the B-V (Brunt-Vaisala) frequency N for an ensemble of stations near Bermuda. At mid-Sargasso Sea sites the dependence was less clear, and showed sensitivity to infrequent large events. Gulf Stream sites showed no abnormally high values of the dissipation.

Oakey (1982) made simultaneous measurements of temperature and velocity gradients in the upper 100 m at the JASIN site (49°N. 15°W); his maximum shears were of the order of 2×10^{-3} sec^{-1}. Oakey and Elliot (1982) performed a week-long study of the mixed layer on the continental shelf off Nova Scotia, and studied the vertical distribution of both shear and Richardson number, Ri. Maximum shear in this region was found to be $\sim 3 \times 10^{-2}$ sec^{-1}. Depending on the drop station, this maximum occurred between 5-15 m depth. They also examined the statistics of Ri occurrence. The depth above which Ri=1 seemed to vary with the inertial period; averaged over 100 determinations, the most probable value of Ri was found to be 10 with transition at 10-25 m from Ri=0.25 to 10.

Patterson, Newman, and Lambert (1981) and Patterson, et al. (1981) performed a statistical analysis of 15 vertical profiles of density and velocity obtained in various ocean areas with a sensor package called YVETTE. Most of the measurements were below a depth of 150 m, i.e. below the mixed layer, and the longest series of observations was 78 hours (h). They could not demonstrate the universality of the Ri distribution, though the profiles had qualitative similarities. They found trends in the spatial distribution of the mean values of Ri. Hebenstreit and Grabowski (1981) have shown that X^2 probability distribution was physically reasonable for the shear values derived from the data set.

D'Asaro and Sanford (1981) measured a longer but discontinuous time series of shear ranging over 14 days during the STREX experiment (near Ocean Station Papa, 50°N, 145°W), and found peak values of 3×10^{-2} sec^{-1}. Perkins and Saunders (1982) using an acoustic three axis current meter (Perkins, et al., 1980) measured shear in the western equatorial Atlantic.

The results of several numerical studies have shown success in the prediction of shear associated with inertial and Ekman currents. Warn-Varnas, Dawson, and Martin (1981) and Davis, et al. (1981) modeled the mixed layer evolution during the MILE experiment (August-September 1977), and computed both mixed layer depths and

vertical distribution of currents that agreed well with experiments. Martin (1982) computed the inertial currents resulting from the passage of Hurricane Eloise in the Gulf of Mexico over the NOAA buoy EB-10. He obtained detailed agreement of both magnitude and phase between observed and computed currents.

3. Modeling Approach

After a survey of the available mixed layer models and models for the seasonal thermocline, we selected the TOPS model currently operational at FNOC. The main ingredient of this model is the Level II turbulence closure model of Mellor and Yamada (1974), which has been extensively tested against observations (Warn-Varnas, Dawson, and Martin (1981), Warn-Varnas and Dawson (1981) and Martin (1982, 1983)) at specific experimental and weather ship locations. It has been tested in an operational sense by Clancy and Martin (1979), Clancy, et al. (1981b), and Clancy and Pollak (1983). In these studies, the TOPS predicted SST (sea surface temperature) and MLD (mixed layer depth) gave rms values much closer to observations than did the climatological values. Comparable comparisons of TOPS predicted shear versus observations were not performed due to the lack of appropriate shear observations for those time periods studied. The model is driven by surface atmospheric stress and heat fluxes derived from the Navy's operational weather prediction models, and initialized by the EOTS (Expanded Ocean Thermal Structure) analysis scheme that blends daily XBT observations with climatology.

For details of the Mellor-Yamada turbulence model and of the TOPS real-time mixed layer model, the reader is referred to the above-mentioned references; only a brief description of these models is given here. The Level-II turbulence closure theory is used to parameterize the vertical eddy fluxes of temperature, salinity and momentum. The essence of this parameterization is the definition of eddy diffusion coefficients based on the turbulent kinetic energy, a turbulence length scale, and empirically derived stability functions. Another important feature of this model is the cut-off of turbulence at the critical Richardson number R_c. Though R_c is normally taken to be 0.25, based on theoretical considerations and the results of certain laboratory experiments, it was found during mixed layer simulations at weather ship sites that sometimes higher values yielded better agreement of model data with observations (e.g. R_c =0.7 at Station Papa in the North Pacific).

The TOPS model is essentially a 3-D mixed layer model based on the turbulence model previously described. It consists of a grid of N quasi-independent mixed layer profiles, but with advection of temperature and salinity between grid points included. The version employed in these studies has been described in detail by Warn-Varnas, et al. (1983) who used it to predict large-scale thermal anomalies in the North Pacific. In this version a stretched vertical grid was used, with Δz = ranging from 5 m near the surface to Δz = 100 m between 300 m and 500 m depth (Fig. 1). The horizontal grid is a rectangular subset of the standard FNOC 63 x 63 Northern Hemisphere Polar Sterographic Grid, with grid spacing at 60°N of Δx = 380 km. The advection current used was the instantaneous wind-drift current containing only the inertial and Ekman components.

The bottom boundary conditions specify constant values of temperature, salinity and velocity. The surface boundary conditions specify fluxes of heat, moisture and momentum. The lateral boundary conditions specify zero fluxes of mass, heat, and salt.

4. Set-Up of Numerical Experiments

At the time these modeling experiments were performed, no velocity fields from the TOPS model were being archived at FNOC. Instead, the TOPS model was installed on the TI/ASC (Texas Instruments/Advanced Scientific computer) in Washington and the model was run continuously in a hindcast mode for 60 days. In regions where the initial profiles are obtained from objective analysis schemes rather than direct ship- or buoy-based observations, an adjustment process takes place because the analyzed fields, heavily weighted in favor of climatology, are not in mechanical and thermodynamic balance with the atmospheric forcing. The "spin-up" time for this adjustment process has been found to be ~15 days and is related to the damping time of inertial oscillations (Niiler and Kraus (1977)). Currently, the forecast fields from the TOPS model are used to provide "first guess" fields for the analysis scheme to reduce the "initialization shock", but for the experiments presented here this improvement was not available. Therefore, we have omitted in our statistical analyses, the first 15 days of the calculations.

Along with the TOPS models, the required atmospheric forcing functions and thermal structure analysis were also set up on the TI/ASC as data banks for various

ocean forecasting and shear calculations. We chose to forecast shear for two 12 x 21 point subregions of the FNOC 63 x 63 grid: one over the north Atlantic and one over the north Pacific (Fig. 2). Two 60 day time periods were used: 28 October through 28 December of 1976 and 1980. Initializing, with a monthly climatological salinity for October and analyzed 28 October thermal structure, TOPS ran 60 days using appropriate FNOC 6 hourly winds and heat flux fields.

The FNOC OTS (Ocean Thermal Structure) and updated EOTS (Extended Ocean Thermal Structure) products provided the thermal structure initialization fields for 1976 and 1980, respectively. Table I lists the FNOC forcing fields required, their source and frequency of record.

From hourly TOPS output, a separate program calculated scalar shear and Richardson number, defined as $S = ((du/dz)^2 + (dv/dz)^2)^{1/2}$ and $Ri = -(g\, d\rho/dz)/\rho S^2$, respectively. Here u and v are the x and y components of velocity and dz represents the vertical distance between given velocity levels. Density is represented by ρ and g is gravitational acceleration S is calculated at velocity levels and Ri at intermediate levels (where ρ is defined).

5. Results and Discussion

In the results to follow, we present contour plots and frequency distributions of S and Ri for various levels and vertical cross-sections within the two domains. The purpose is to investigate horizontal, vertical, and temporal variability, as well as any relations to geography and synoptic weather events, that might be extracted from potential FNOC shear products. To support our choice of product displays, we shall give a brief discussion of mixed layer physics and associated shears and Richardson numbers.

a. Mixed Layer Evolution and Shears: The typical density structure in the upper layers of the ocean consists of a pycnocline with an isopycnal mixed layer above and a dynamically stable water mass below. The vertical uniformity of the mixed layer results from stirring caused by wind induced shear instabilities and surface cooling induced penetrative convection. In the stable water mass below, the vertical eddy fluxes are small. During strong wind forcing or strong surface cooling, mixed layer deepening occurs due to entrainment from below caused by turbulent mixing. During

weak wind forcing and strong surface heating, the decrease in turbulent kinetic energy results in insufficient mixing to diffuse heat downward, and a warm stratified surface layer forms which eventually becomes another mixed layer. At times therefore, the upper layer of the ocean may have a multiple mixed layer structure. The currents within the mixed layer presently predicted by TOPS combine Ekman and inertial components. One might expect, under weak winds or relatively strong heating, Ekman currents to dominate with the resultant shear decreasing from the surface to the base of the mixed layer. With strong and variable winds (such as storm passage) or surface cooling, the mixed layer will homogenize, acting as a uniformly mixed slab yielding strong inertial shear at the base of the mixed layer. Between these extremes lie various combinations of Ekman plus inertial current produced shear, throughout the mixed layer.

The parameter which measures that tendency for stratified shear flows to become unstable is the Richardson number, Ri. Based on theoretical predictions and laboratory observations shear instability occurs for the range $0 \leq Ri \leq 0.25$; with negative values corresponding to convective instability and values > 0.25 corresponding to stable flow.

In the figures shown later, the Ri plots show regions of shear instability ($0 \leq Ri \leq 0.25$) by shading. The obvious break between stable waters below the pycnocline and generally unstable waters above shows up in the vertical cross-sections of Ri. In the shear cross-sections the base of the mixed layer appears as an occasional tendency toward a primary or secondary shear maximum.

One can anticipate four relevant time scales, corresponding to the four dominant time scales of the atmospheric forcing functions. A diurnal scale may result from the diurnal heating-cooling cycle. A synoptic (3-7 day) scale should result from the aperiodic progression of fronts and storms through the regions. A seasonal scale might emerge due to the seasonal variation of the atmospheric forcing. An inter-annual scale might also appear due to year-to-year changes in storm frequency, tracks and intensity. We do not expect to see any seasonal variation in our results due to our looking only at fall time periods.

b. Diurnal Variation: We shall first look at 6-hourly snapshots of shear and Ri distributions in the North Pacific for the 13 November 1976. Figure 3 illustrates

contours of Ri at 10 m depth, and Figure 4 contours of shear at 7.5 m depth. These snapshots demonstrate a high degree of variability just within one day. This probably results from diurnal variability in solar heating combined with synoptic scale weather changes. There appears to be a decrease in areas of shear instability (shaded portions with $0 \leq Ri \leq 0.25$) during the nocturnal hours, and a decrease in high shear regions. Typical shear values average between 4 and 8 x 10^{-3} sec^{-1} over the region, with maximum values greater than 1.2 x 10^{-2} sec^{-1} occurring at noon in a small region at ~180°W. Large areas of negative Ri appear at night, indicating possible convective instability due to nocturnal cooling. Figures 5 and 6 illustrate a roughly meridional cross-section of Ri and S, respectively, from 0-400 m depth along the line C-D in Figure 2. The bottom contour line of Ri = 0.50 is a reasonable indicator of mixed layer depth, since below that Ri increases with increasing water stability. A trend of mixed layer depth increase with decreasing latitude appears, at least down to ~30°N (see Fig. 3(a) for coordinates): There is also a trend to larger mixed layer depths south of 30°N during the night hours; this is possibly due to penetrative convection associated with nocturnal cooling as evidenced by the increased area of negative Ri. The contours of shear appear to center about a point located at the surface near 40°N. There also appear secondary maxima of shear at depths of 35-50 m, with highest values at 6 p.m. local.

To isolate the diurnally forced effects, we averaged the 1976 north Pacific results over the final 45 days comparing mean shear for local noon, local midnight and overall values for both C-D (Fig. 7) and A-B (Fig. 8) cross-sections. The nocturnal decrease in shear again shows up south of 30° but other than this any diurnal effect appears minimal. These average results are consistent with the earlier observation that mixed layer depth increases with decreasing latitude, down to ~30°N, where there is an abrupt shallowing. These trends are consistent with Ekman convergence causing a southward mixed layer deepening with an abrupt shallowing at the subtropical convergence. The subtropical convergence should occur around 30°N at this location for this time of year but with displacements of up to ten degrees latitude expected within four weeks time (Roden, 1975).

Another point is the high variability shown by the deviation on the overall mean. Minimal diurnal variability combined with the high variability shown by the overall deviation together suggest the major importance of another time scale. Figures 9 and 10 display the average diurnal variation in the North Atlantic, with

similar results. In conclusion, our results indicate, for our study periods and regions, that diurnal effects on the distribution and statistics of shear and Richardson number are small.

c. Synoptic Variation: We will examine the effects of synoptic weather on the distribution of shear and Richardson number by displaying intensity contours and probability distributions. Figures 11 and 12 show contours of Ri at 10 m and S at 7.5 m, respectively for local noon of 13, 15, 17, and 19 November. Looking at this specific time sequence limits the generality of our conclusions but leaves in the variability wiped out by averaging. We note that a "tongue" of very low shear shows up on 17 November around 160°W, coinciding with a large tongue of negative Ri where presumably penetrative convective cooling is present. There appears to be no systematic trend in the size and location of the shaded regions where $0 \leq Ri \leq 0.25$, i.e. where shear instability prevails. In general, almost half the Pacific region on 13 and 17 November appears subject to shear instability but only a quarter or so on 15 amd 19 November. Later we make comparisons with the corresponding synoptic weather charts to explain the peculiar varability displayed in this sequence of snapshots.

Figures 13 and 14 show roughly meridional distributions for Ri and S, respectively, along C-D cross-sections for 13, 15, 17, and 19 November. Again note the increase of mixed layer depth with decreasing latitude, and the sudden shallowing south of 30°N on 13 and 15 November. The shallowing is missing on 17 November and a large region of shallow mixed layer depth develops between 30°N and 44°N on 19 November. Below 15 m depth Ri is negative, indicating the presence of remnant convective instability from the previous day.

What caused the high day to day variability seen in both the shear and Ri plots? Halpern (1974) found dynamic stability in the mixed layer, affected by frontal passage. Using a mooring in the Northeastern Pacific, a 30 day data series indicated the onset of shear instability in the surface layers apparently related to a passing front. Likewise, in our model results, the regions of shear instability appear directly correlated to frontal passage (Fig. 15). Convective instability appears just after frontal passage, and regions of stability occur under high pressure systems with their expected lower wind speeds and reduced cloud cover. The rapid transition of highly unstable to highly stable conditions at 10 m between 17 and 19

November 1976 (Fig. 15 c, d) shows up as just a surface phenomenon in the C-D cross-section (Fig. 13) and is apparently due to rapid surface heating linked to the progress of a high pressure system through the region.

An interesting geographic variability occurs in the 1976 C-D shear cross-section (Fig. 14). D'Asaro and Sanford (1981) recorded shear peaks at the base of the mixed layer in their 1980 Ocean Station Papa work. Papa's position occurs on the left side of the C-D x-section plots. Model results for 1976 and 1980 also yield shear maxima at the pycnocline in the northern region (left side). However, this pycnocline maximum decreases or disappears toward the south. Low pressure passage through the ocean station region on the 13th and 15th (top of Fig. 15) appears the likely cause of the model's northerly pycnocline shear maximum. A comparison of Figures 14 and 15 suggest that the maxima at the pycnocline may result from the direct overhead passage of low pressure centers. As mentioned earlier, the high winds associated with the storm passage would be expected to homogenize the mixed layer, probably setting up strong inertial shear at the pycnocline as the storm passed. The occurrence of pycnocline shear maxima to the north rather than the south is reasonable, given the favored northerly storm tracks in this region.

A more direct way of seeing the wind forcing/shear connection appears in the Figure 16 phase plots. C-D cross-sections of wind speed, 7.5 m shear, and 32.5 m shear are juxtaposed and plotted at twelve hour intervals for 24 days. The results demonstrate the strong qualitative correlation between wind forcing and resultant near surface and near pycnocline shear.

For the 7 day period just discussed, values of near surface and near-pycnocline Ri and S over the entire North Pacific region are available from the histograms of Figures 17-20. Distributions of Ri at both 10 and 36.3 m suggest the high incidence of shear instability ($0 \leq Ri \leq 0.25$). Near surface (7.5 m) shear values range primarily between 10^{-3} and 10^{-2}/s. The majority of near pycnocline values occur between 10^{-3} and 5×10^{-3}/s.

Figures 21-25 yield a synoptic-scale picture for the North Atlantic comparable to the Pacific. As in the Pacific results, the highest variability appears associated with synoptic weather patterns rather than with diurnal changes. 10 m Ri, 7.5 m shear, and G-H cross-sections of both (Figs. 21-24), demonstrate this variability.

Plots for 12-18 November 1976 (Fig. 25) show regions of shear instability and high shear again generally tracking with frontal passage. Convectively unstable low shear regions again appear behind the fronts. The definite shear maxima at the mixed layer base again occur primarily to the north (right side of Fig. 24) associated with the Icelandic low.

d. Interocean Comparison: We now consider the variability of significant shear for local noon 12-18 November for the Atlantic and Pacific at 7.5 and 32.5 m (Fig. 26). Note that the surface layers have higher shear than that near the base of the mixed layer and that high day-to-day variability occurs for this particular time period. Higher percentages of significant shear appear in the north Pacific than in the north Atlantic but given the limited time average and regional space averages, this result is inconclusive.

To actually perform a more reasonable inter-ocean comparison, we plotted cumulative hourly Ri and S from mid-November through December 1976 (Figs. 27, 28). We used mid-ocean points at 45° in the Pacific and Atlantic, at near-surface and near-pycnocline depths. Ri appears skewed toward convective instability in the surface layer. Surface shear, besides being much higher in both cases, shows a slight and a definite bi-modal distribution in the Pacific and the Atlantic, respectively. The bulk of the Pacific surface shear occurs around 5×10^{-3} s^{-1} with a suggestion of a secondary peak near $10^{-2}s^{-1}$ while the dominant Atlantic surface shear peaks at $10^{-3}s^{-1}$ with a secondary peak at $8 \times 10^{-3}s^{-1}$. Increases and decreases of wind associated with weather systems may cause this bimodality in shear as the model shifts between dominant Ekman shear and dominant inertial shear modes.

e. Interannual Variability: Year to year variations in storm frequency, intensity and tracks might cause shear variation on an interannual scale. C-D and A-B cross-sections of 45 day mean shear and standard deviation demonstrate the effects of this variability (Figs. 29-30). The tendency for shear maxima at the pycnocline again shows up in the mean plots for 1976 and 1980 with the strongest indications to the north (left side of Fig. 29). A preferred southerly storm track, a major storm or storms, or stalling of a storm is suggested at about 40°N in 1980, given the high mean shear appearing near the middle in both 1980 cross-sections.

6. Summary and Conclusions

In an effort to demonstrate the shear prediction capabilities of TOPS at FNOC, we attempted to simulate the statistics of temporal and geographical distribution of shear and Richardson number in the upper 400 m of the world's oceans. Specifically, we examined two 60 day periods in October-November of 1976 and 1980, for large areas of the North Pacific and North Atlantic. The atmospheric driving forces were derived from prediction fields obtained from Fleet Numerical Oceanography Center's hemispheric weather prediction models. Some of the results for our particular periods and areas of study can be summarized as follows:

(a) High shear variability appears on diurnal, synoptic, and interannual time scales. This result suggests the preferability of forecast shear over climatological values for operational applications even if climatological values were available.

(b) Diurnally forced variability appears only weakly except south of 30°N.

(c) Shear maxima are usually located near the surface with secondary maxima appearing near the base of the mixed layer. However, more consistent with observations, primary maxima at the mixed layer base appear linked with storm passage.

(d) High spatial and temporal variability of both S and Ri appear qualitatively correlated with the periodic passage of synoptic weather patterns. Within the mixed layer, the onset of shear instability coincides with atmospheric frontal passage; convective instability appears immediately following frontal passage; and stable conditions are associated with high pressure systems.

Plots for 12-18 November 1976 (Fig. 25) show regions of shear instability and high shear again generally tracking with frontal passage. Convectively unstable low shear regions again appear behind the fronts. The definite shear maxima at the mixed layer base again occur primarily to the north (right side of Fig. 24) associated with the Icelandic low.

d. Interocean Comparison: We now consider the variability of significant shear for local noon 12-18 November for the Atlantic and Pacific at 7.5 and 32.5 m (Fig. 26). Note that the surface layers have higher shear than that near the base of the mixed layer and that high day-to-day variability occurs for this particular time period. Higher percentages of significant shear appear in the north Pacific than in the north Atlantic but given the limited time average and regional space averages, this result is inconclusive.

To actually perform a more reasonable inter-ocean comparison, we plotted cumulative hourly Ri and S from mid-November through December 1976 (Figs. 27, 28). We used mid-ocean points at 45° in the Pacific and Atlantic, at near-surface and near-pycnocline depths. Ri appears skewed toward convective instability in the surface layer. Surface shear, besides being much higher in both cases, shows a slight and a definite bi-modal distribution in the Pacific and the Atlantic, respectively. The bulk of the Pacific surface shear occurs around 5×10^{-3} s^{-1} with a suggestion of a secondary peak near $10^{-2}s^{-1}$ while the dominant Atlantic surface shear peaks at $10^{-3}s^{-1}$ with a secondary peak at $8 \times 10^{-3}s^{-1}$. Increases and decreases of wind associated with weather systems may cause this bimodality in shear as the model shifts between dominant Ekman shear and dominant inertial shear modes.

e. Interannual Variability: Year to year variations in storm frequency, intensity and tracks might cause shear variation on an interannual scale. C-D and A-B cross-sections of 45 day mean shear and standard deviation demonstrate the effects of this variability (Figs. 29-30). The tendency for shear maxima at the pycnocline again shows up in the mean plots for 1976 and 1980 with the strongest indications to the north (left side of Fig. 29). A preferred southerly storm track, a major storm or storms, or stalling of a storm is suggested at about 40°N in 1980, given the high mean shear appearing near the middle in both 1980 cross-sections.

6. Summary and Conclusions

In an effort to demonstrate the shear prediction capabilities of TOPS at FNOC, we attempted to simulate the statistics of temporal and geographical distribution of shear and Richardson number in the upper 400 m of the world's oceans. Specifically, we examined two 60 day periods in October-November of 1976 and 1980, for large areas of the North Pacific and North Atlantic. The atmospheric driving forces were derived from prediction fields obtained from Fleet Numerical Oceanography Center's hemispheric weather prediction models. Some of the results for our particular periods and areas of study can be summarized as follows:

(a) High shear variability appears on diurnal, synoptic, and interannual time scales. This result suggests the preferability of forecast shear over climatological values for operational applications even if climatological values were available.

(b) Diurnally forced variability appears only weakly except south of 30°N.

(c) Shear maxima are usually located near the surface with secondary maxima appearing near the base of the mixed layer. However, more consistent with observations, primary maxima at the mixed layer base appear linked with storm passage.

(d) High spatial and temporal variability of both S and Ri appear qualitatively correlated with the periodic passage of synoptic weather patterns. Within the mixed layer, the onset of shear instability coincides with atmospheric frontal passage; convective instability appears immediately following frontal passage; and stable conditions are associated with high pressure systems.

FNOC Fields Used for TOPS Forcing

Field	Source	Frequency
Boundary Layer Wind Speed	Planetary Boundary Layer Model	6 hourly
Boundary Layer Wind Direction	Planetary Boundary Layer Model	6 hourly
Solar Radiation Flux	Primitive Equation Model	6 hourly
Total Heat Flux	Primitive Equation Model	6 hourly
Evaporative Heat Flux	Primitive Equation Model	6 hourly
Precipitation	Primitive Equation Model	12 hourly

REFERENCES

Clancy, R. M. and P. J. Martin, 1979: The NORDA/FLENUMOCEANCEN thermodynamical ocean prediction system (TOPS): A technical description. NORDA Tech. Note 54, 28 p.

Clancy, R. M. and P. J. Martin, 1981: Synoptic forecasting of the oceanic mixed layer using the Navy's operational environmental data base: Present capabilities and future applications. Bull. Amer. Met. Soc., 62, p. 770-784.

Clancy, R. M., P. J. Martin, S. A. Piacsek, and K. Pollak, 1981(a): The current state of ocean thermal forecasting at FNOC. In Ocean Prediction: The Scientific Basis and the Navy's Needs, Proc. of the Ocean Prediction Workshop, Monterey, CA, May 1981, p. 186.

Clancy, R. M., P. J. Martin, S. A. Piacsek and K. D. Pollack, 1981(b): Test and evaluation of an operationally capable synoptic upper-ocean forecast system. NORDA Tech. Note 92, 66 p.

Clancy, R. M. and Pollak, K., 1983: A real-time synoptic ocean thermal analysis/ forecast system. Progress in Oceanography, 4, p. 1-42..

Davis, R. E., R. DeSzoeke, D. Halpern, and P. Niiler 1981: Variability in the upper ocean during MILE. Part II: Modeling the mixed layer response. Deep Sea Res. 28A, p. 1453-1475.

D'Asaro, E. and T. B. Sanford, 1981: STREX upper ocean velocity profiles. In Storm Transfer and Response Experiment Workshop Report, U.S. Dept of Commerce.

Evans, D. L., 1982: Observations of small-scale shear and density structure in the ocean. Deep Sea Res., 29, p. 581-595.

Gargett, A. E. and R. R. Osborn, 1981: Small-scale shear measurements during the Fine and Microstructure Experiment (FAME). J. Geophys. Res., 86, p. 1929-1944.

Gargett, A. E., P. J. Hendricks, T. B. Sanford, T. R. Osborn, A. J. Williams III, 1981: A composite spectrum of vertical shear in the upper ocean. J. Phys. Oceanogr., 11, p. 1258-71.

Gregg, M. C. and T. B. Sanford, 1980: Signatures of mixing from the Bermuda slope, the Sargasso Sea and the Gulf Stream. J. Phys. Oceanogr., 10, p. 105-127.

Halpern, D., 1974: Observations of the deepening of the wind-mixed layer in the northeast Pacific Ocean. J. Phys. Oceanogr., 4, p. 454-66.

Hebenstreit, G. T. and W. Grabowski, 1981: Statistical modeling of shear in the upper ocean. Science Applications, Inc., Tech. Report 82-382-WA, March 1981.

Lange, R. E., 1981: Observations of near-surface oceanic velocity strain-rate variability during and after storm events. J. Phys. Oceanogr., 11, p. 1272-1279.

Martin, P. J., 1982: Mixed-layer simulation of buoy observations taken during Hurricane Eloise. J. Geophys. Res., 87, p. 409-427.

Martin, P. J., 1983: Simulation of the mixed layer at ocean weather station November and Papa with several models. NORDA Tech. Report (in preparation).

Mellor, G. L. and T. Yamada, 1974: A hierarchy of turbulence closure models for planetary boundary layers. J. Atmos. Sci., 31, p. 1791-1806.

Niiler, P. P. and E. B. Kraus, 1977: One-dimensional models of the upper ocean. In Modeling and Prediction of the Upper Layers of the Ocean, ed. E. B. Kraus, Pergamon Press, Oxford, p. 143-172.

Oakey, N. S., 1982: Determination of the rate of dissipation of turbulent energy from simultaneous temperature and velocity shear microstructure measurements. J. Phys. Oceanogr., 12, p. 256-271.

Oakey, N. S. and J. A. Elliott, 1982: Dissipation within the surface mixed layer. J. Phys. Oceanogr., 12, p. 171-185.

Patterson, S. L., F. C. Newman, D. M. Rubenstein, and R. B. Lambert, 1981: Spatial distribution of vertical shear. Science Applications, Inc., Tech Report 81-201-02, March 1981.

Patterson, S. L., F. C. Newman and R. B. Lambert, 1981: Observed spatial variations in Richardson Number Statistics. Science Applications, Inc., Tech. Report 82-429-WA, April 1981.

Perkins, H. T., K. D. Saunders, G. Appell and T. Mero, 1980: Design and initial testing of a three-axis current meter. OCEANS '80 Conference Record (IEEE Pub. No. 80CH1572-7), p. 319-322.

Perkins, H. T., K. D. Saunders, 1982: Physical oceanographic observations in the northwest tropical Atlantic. Tropical Ocean-Atmosphere Newsletter, No. 13, p. 7-8.

Roden, G. I., 1975: On North Pacific temperature, salinity, and sound velocity and density fronts and their relation to the wind and energy flux fields. J. Phys. Oceanogr., 5, p. 557-571.

Warn-Varnas, A. C., R. M. Clancy, M. L. Morris, P. J. Martin, S. Horton, 1983: Studies of large-scale thermal variability with a synoptic mixed-layer model. NORDA Tech. Report 156, 34 p.

Warn-Varnas, A. C. and G. Dawson, 1981: An analysis of modeled shear distribution during MILE. NORDA Tech. Note 84, 36 p.

Warn-Varnas, A. C., G. Dawson and P. J. Martin, 1981: Forecast and studies of the oceanic mixed layer during the MILE experiment. Geophys. Astrophys. Fluid Dyn., 17, p. 63-85.

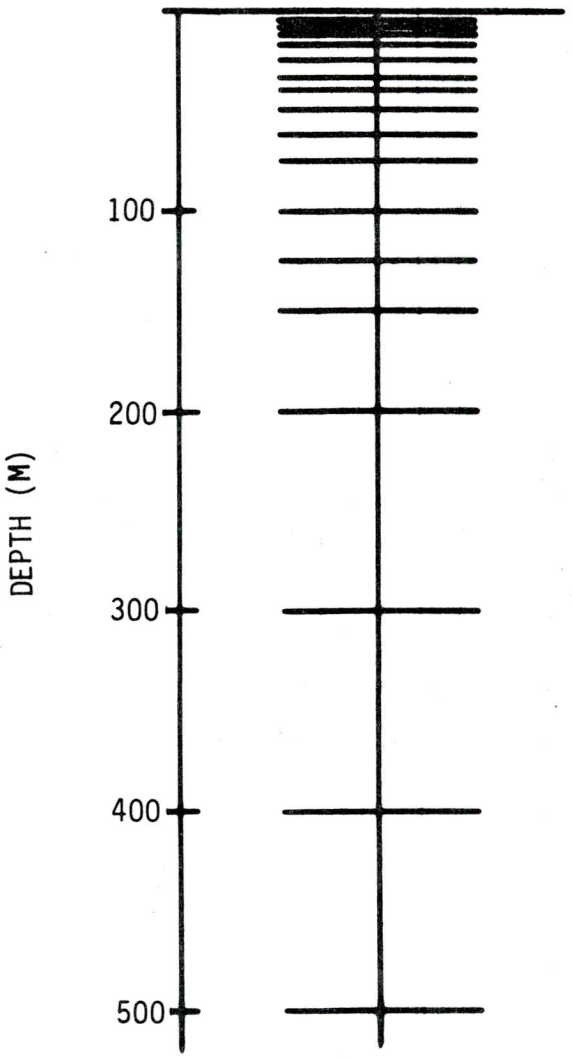

Figure 1. Vertical grid used by TOPS. Quantities $\overline{T}$, $\overline{S}$, $\overline{u}$, $\overline{v}$, u_a *and* v_a *are defined at depths indicated. All turbulence quantities and* w_a *are defined and depths midway between those shown.*

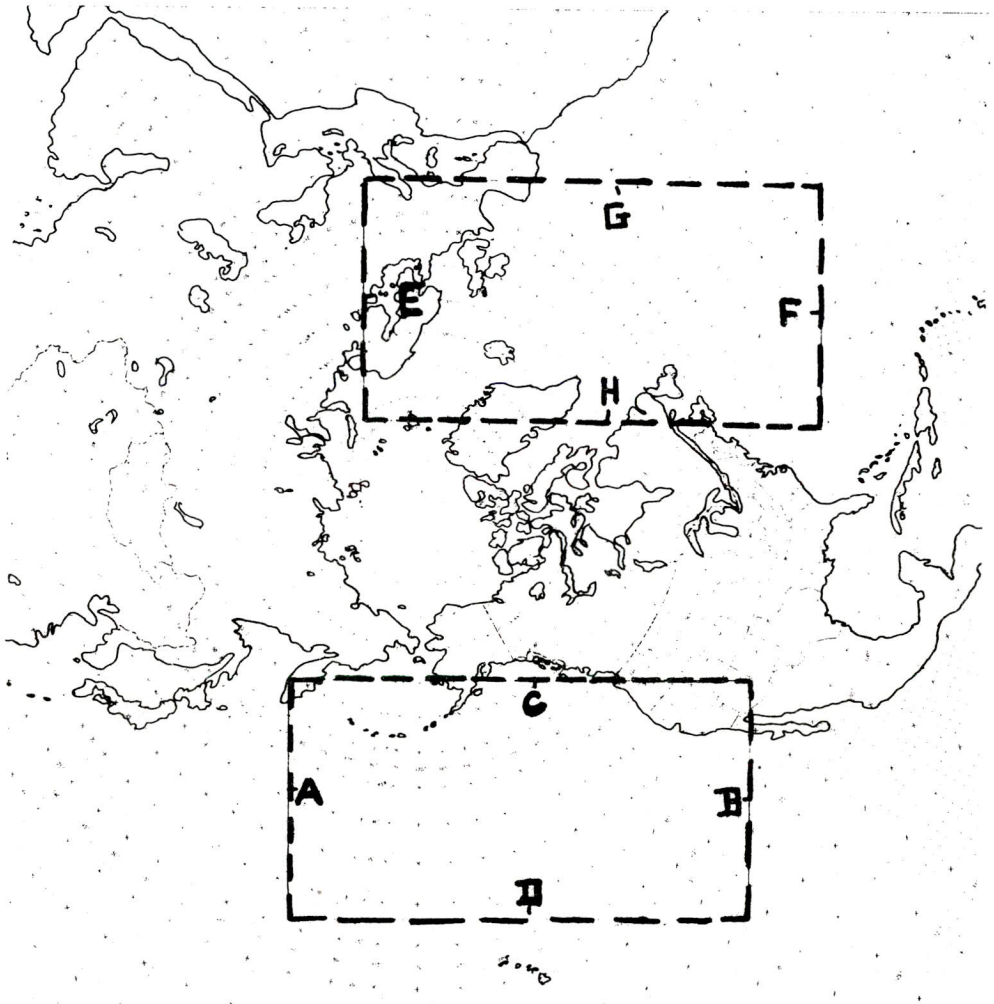

Figure 2. North Pacific and North Atlantic computational domains on the FNOC polar stereographic grid.

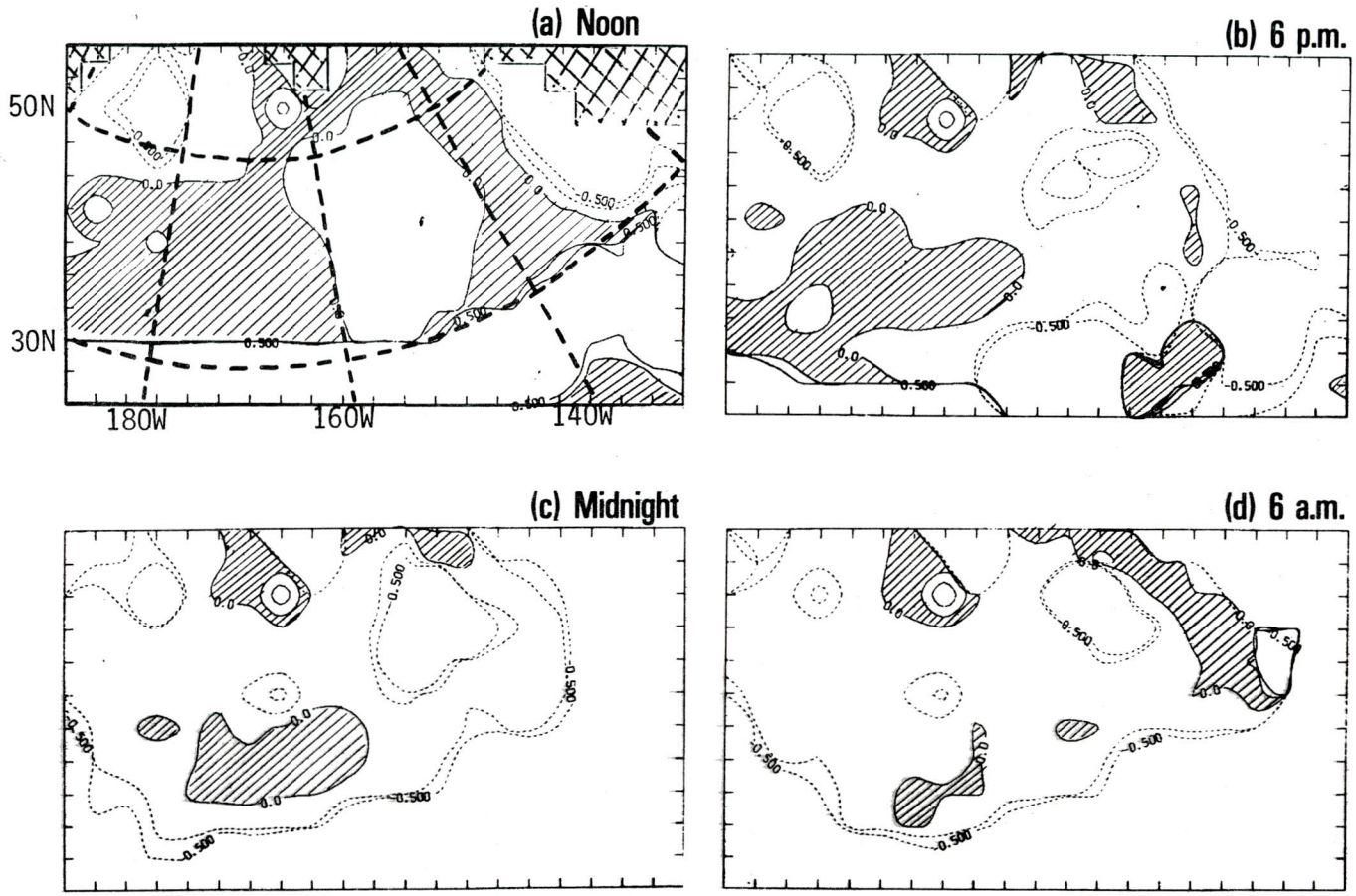

Figure 3. Diurnal variation of 10 m Ri in the North Pacific on 13 Nov 76.

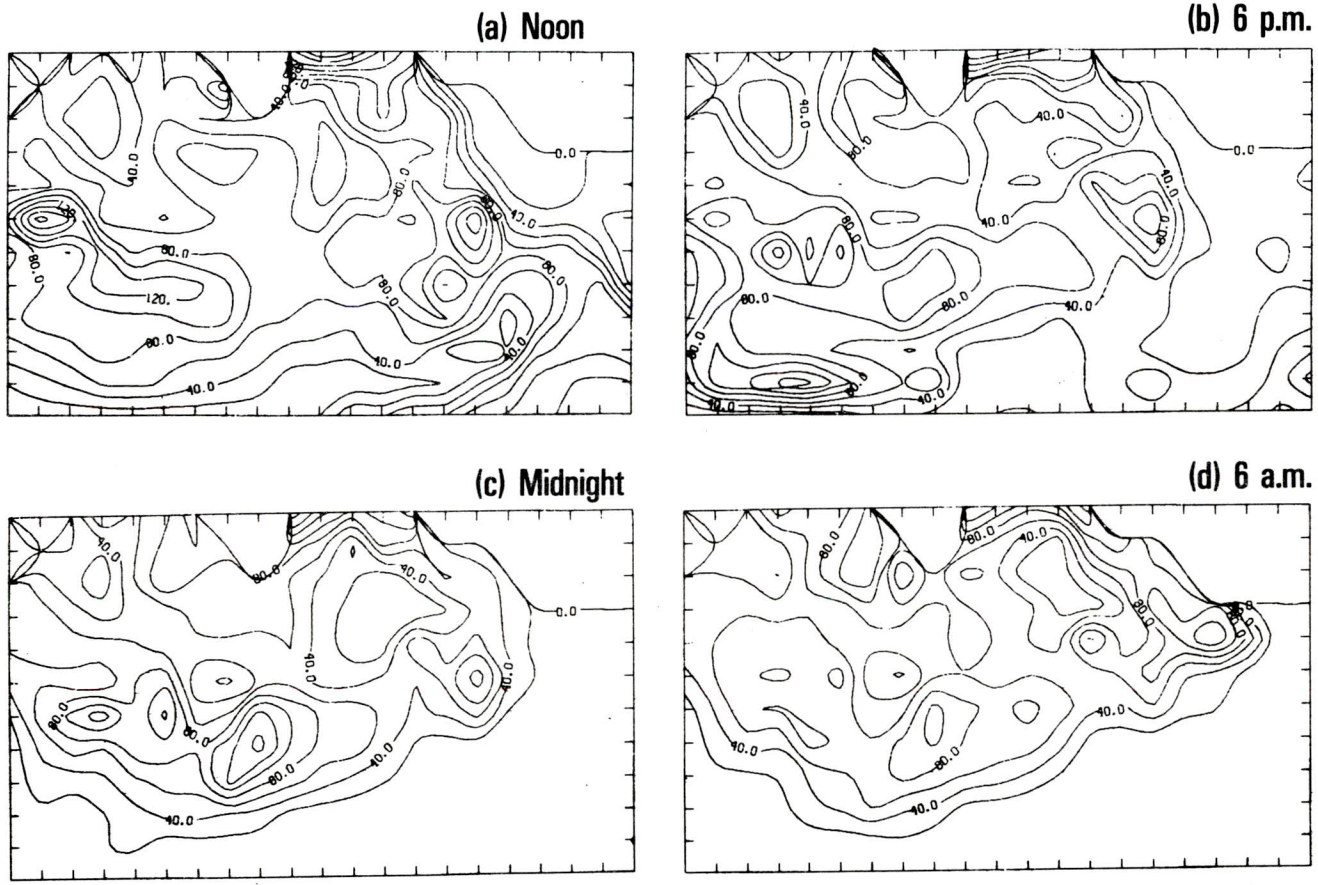

Figure 4. Diurnal variation of 7.5 m shear (s^{-1} x 10^4) in the North Pacific on 13 Nov 76.

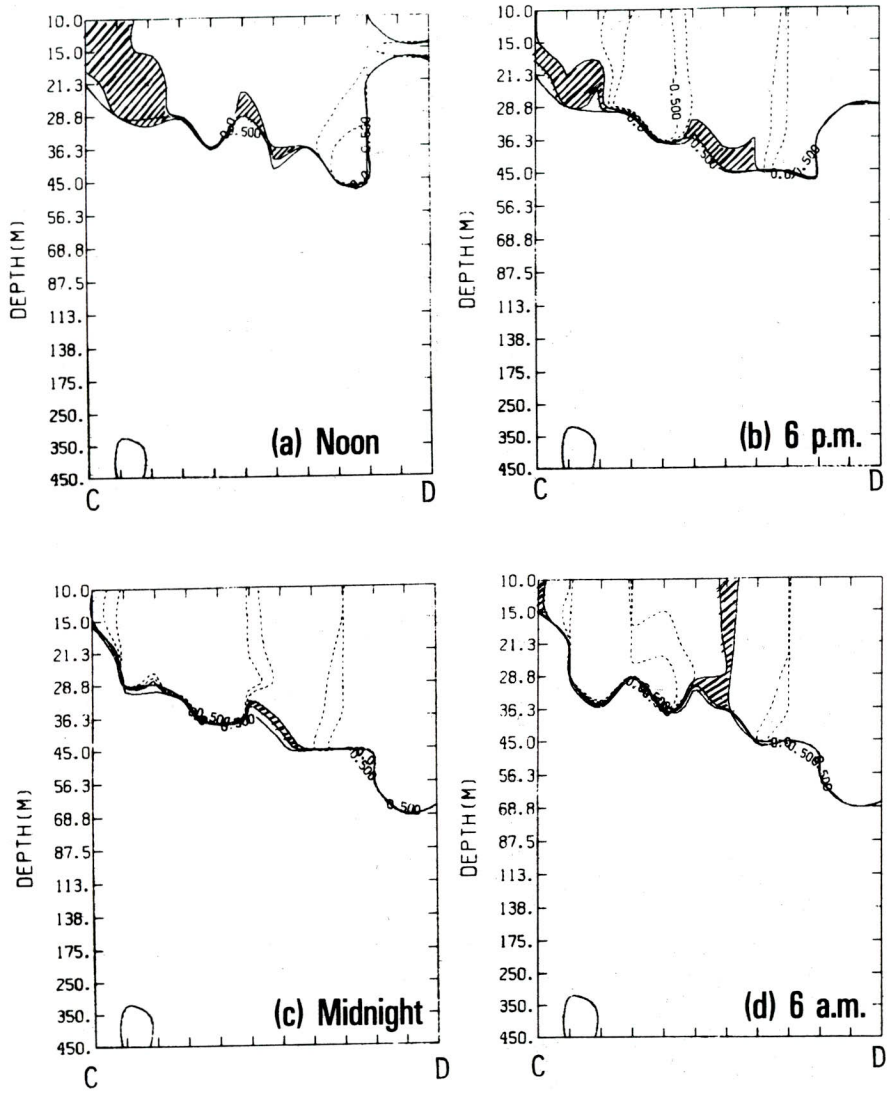

Figure 5. Diurnal variation of Ri along C-D cross section on 13 Nov 76.

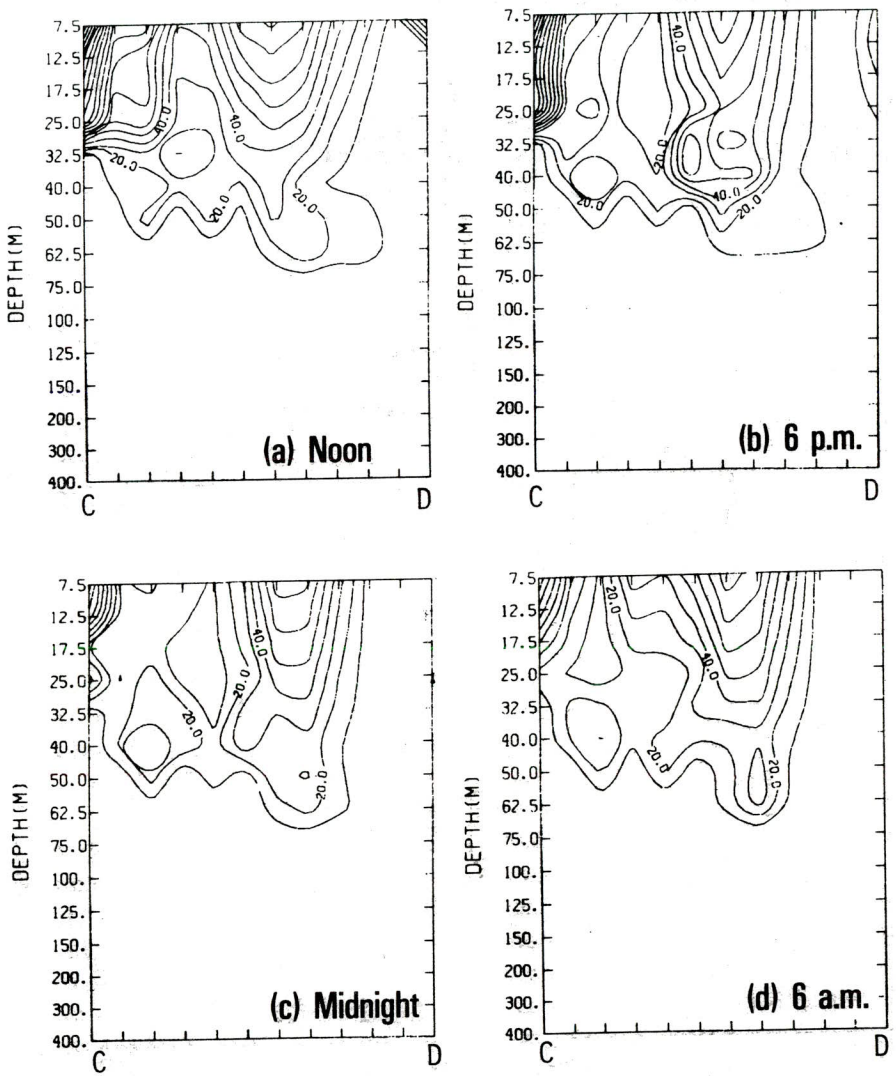

Figure 6. Diurnal variation of shear (s^{-1} x 10^4) along C-D cross-section on 13 Nov 76.

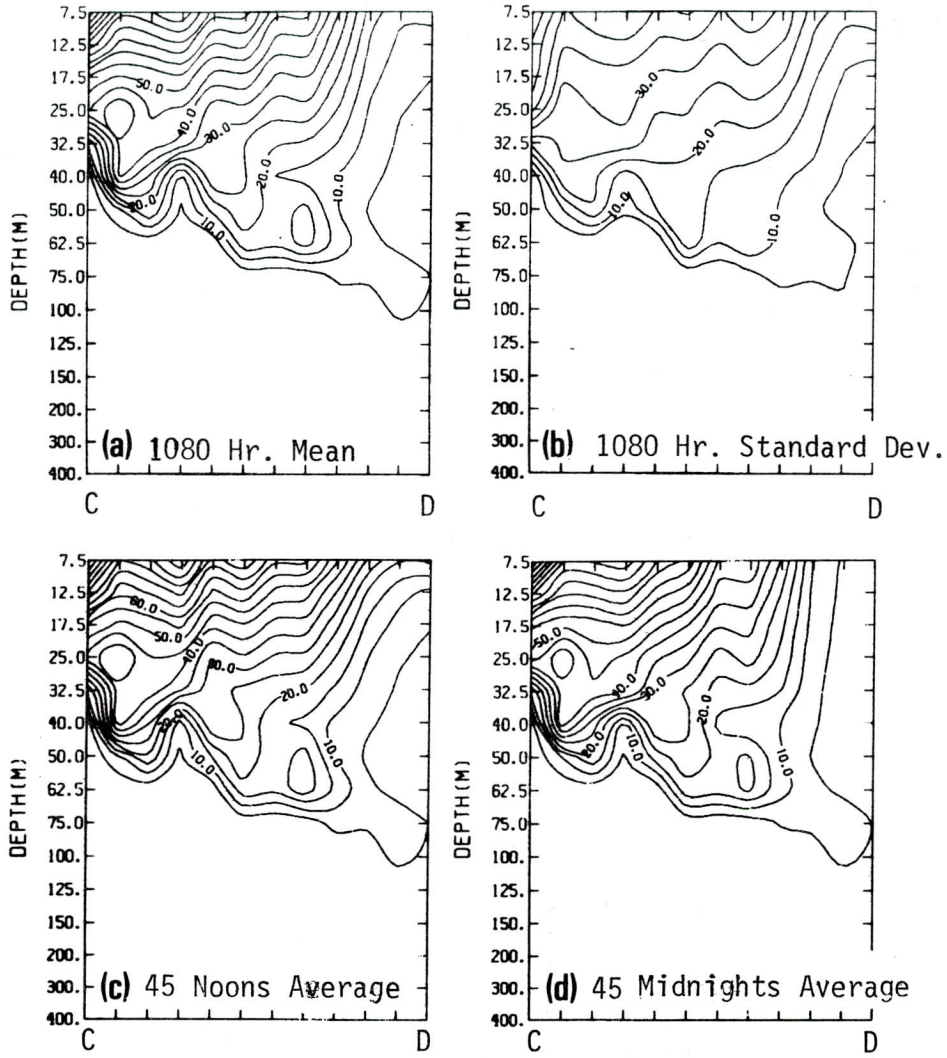

Figure 7. Diurnal variation of shear ($s^{-1} \times 10^4$) along C-D cross-section as shown by the overall Nov-Dec 1976 (a) mean and (b) standard deviation, compared to the (c) noontime and (d) midnight averages.

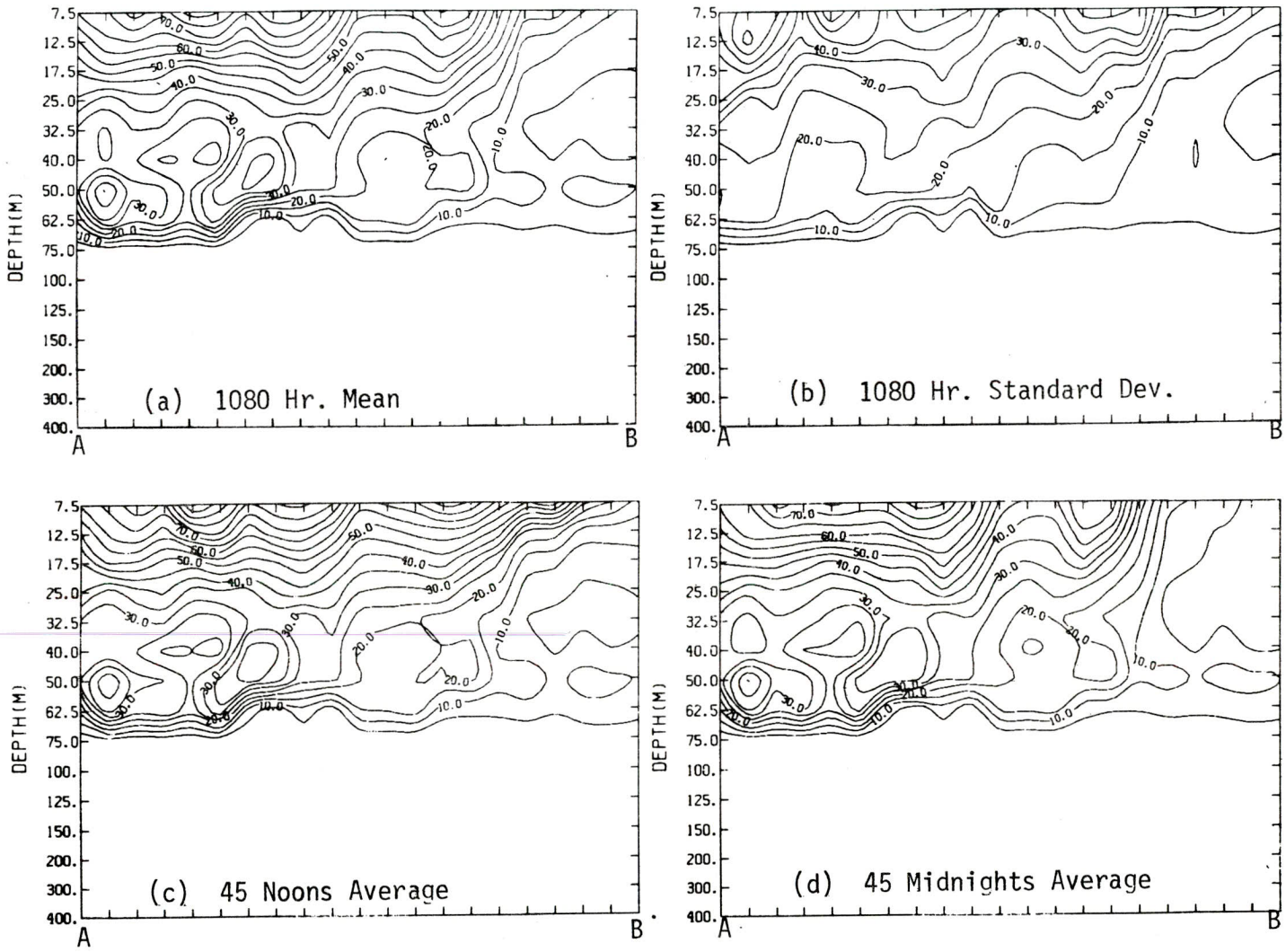

Figure 8. Diurnal variation of shear (s^{-1} x 10^4) along A-B cross-section as shown by the overall Nov-Dec 1976 (a) mean and (b) standard deviation, compared to the (c) noontime and (d) midnight averages.

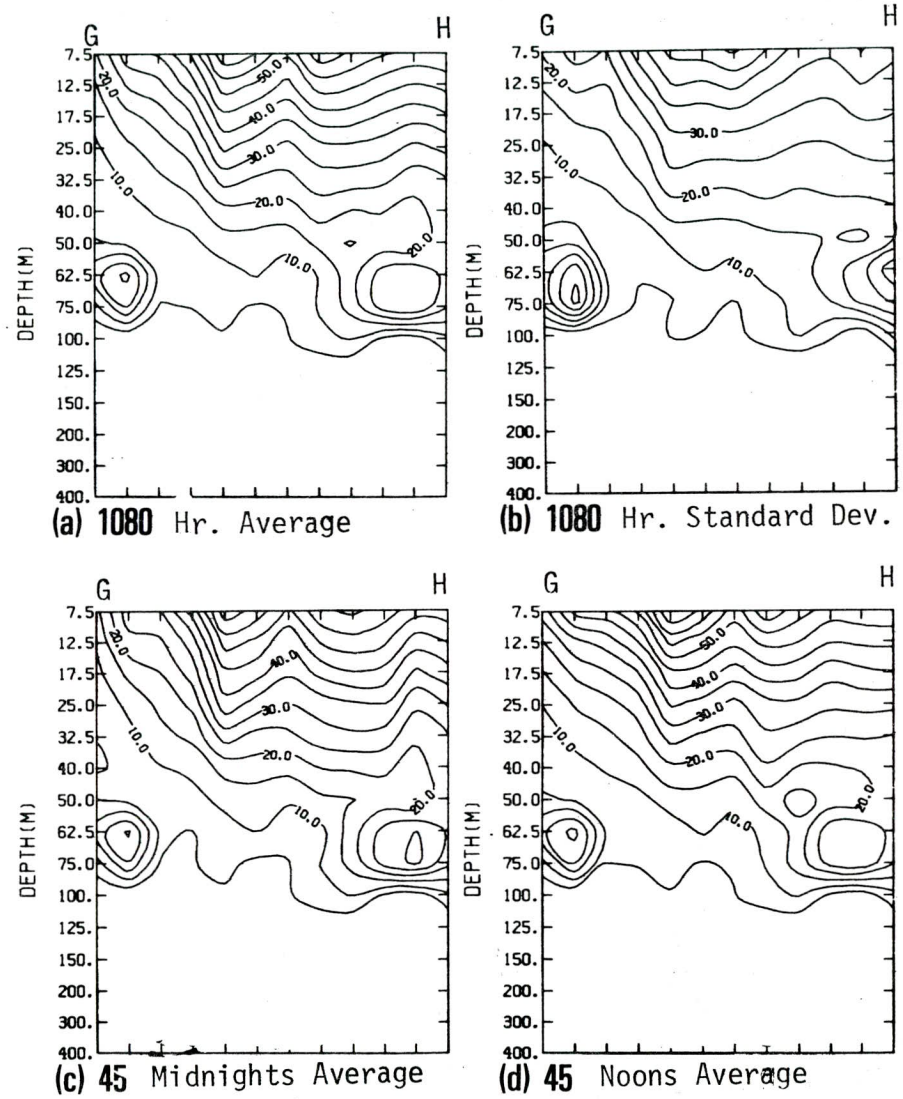

Figure 9. Diurnal variation of shear (s^{-1} x 10^4) along G-H cross-section as shown by the overall Nov-Dec 1976 (a) mean and (b) standard deviation compared to the (c) midnight and (d) noontime averages.

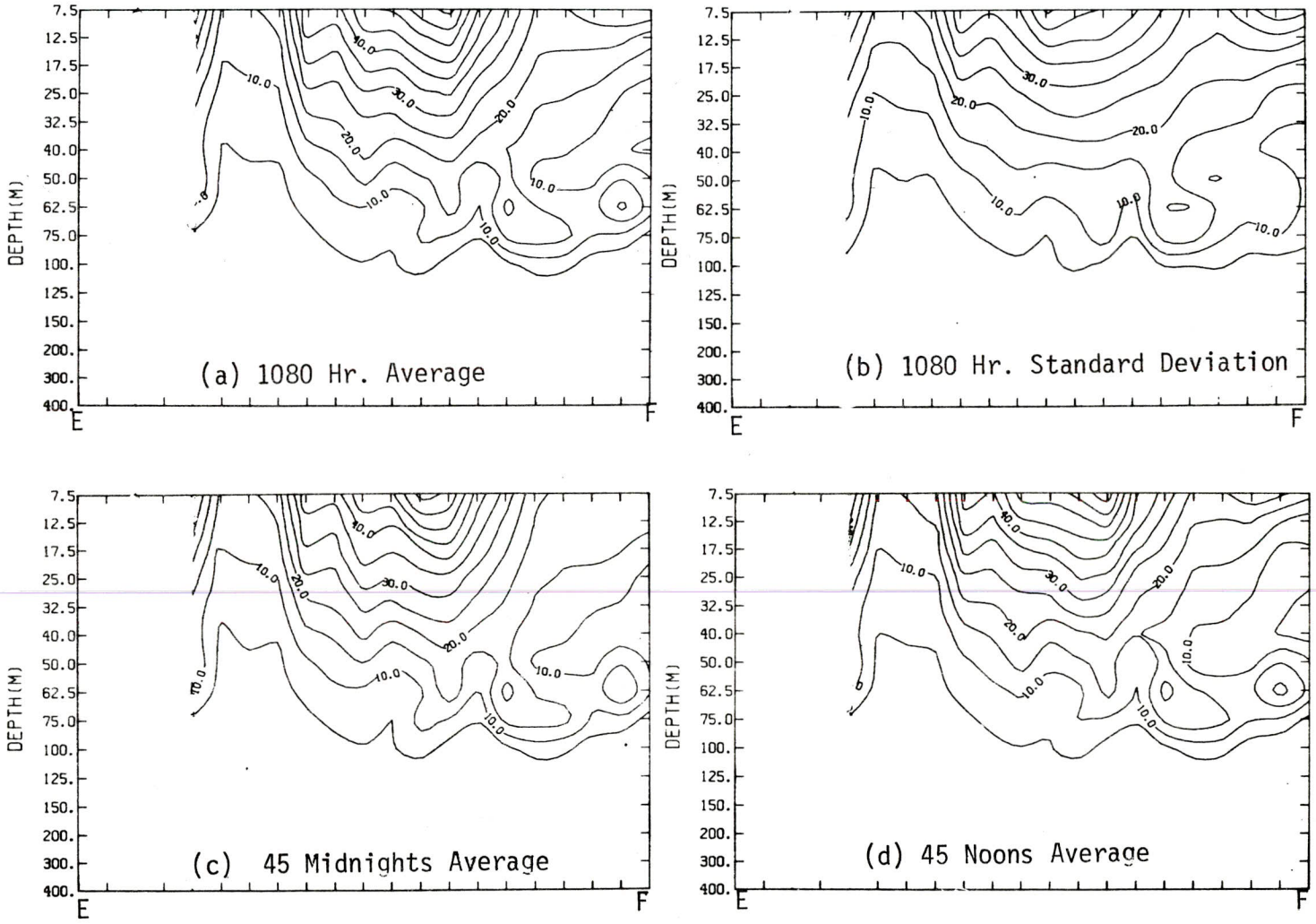

Figure 10. Diurnal variation of shear (s^{-1} x 10^4) along E-F cross-section as shown by the overall Nov-Dec 1976 (a) mean and (b) standard deviation, compared to the (c) midnight and (d) noontime averages.

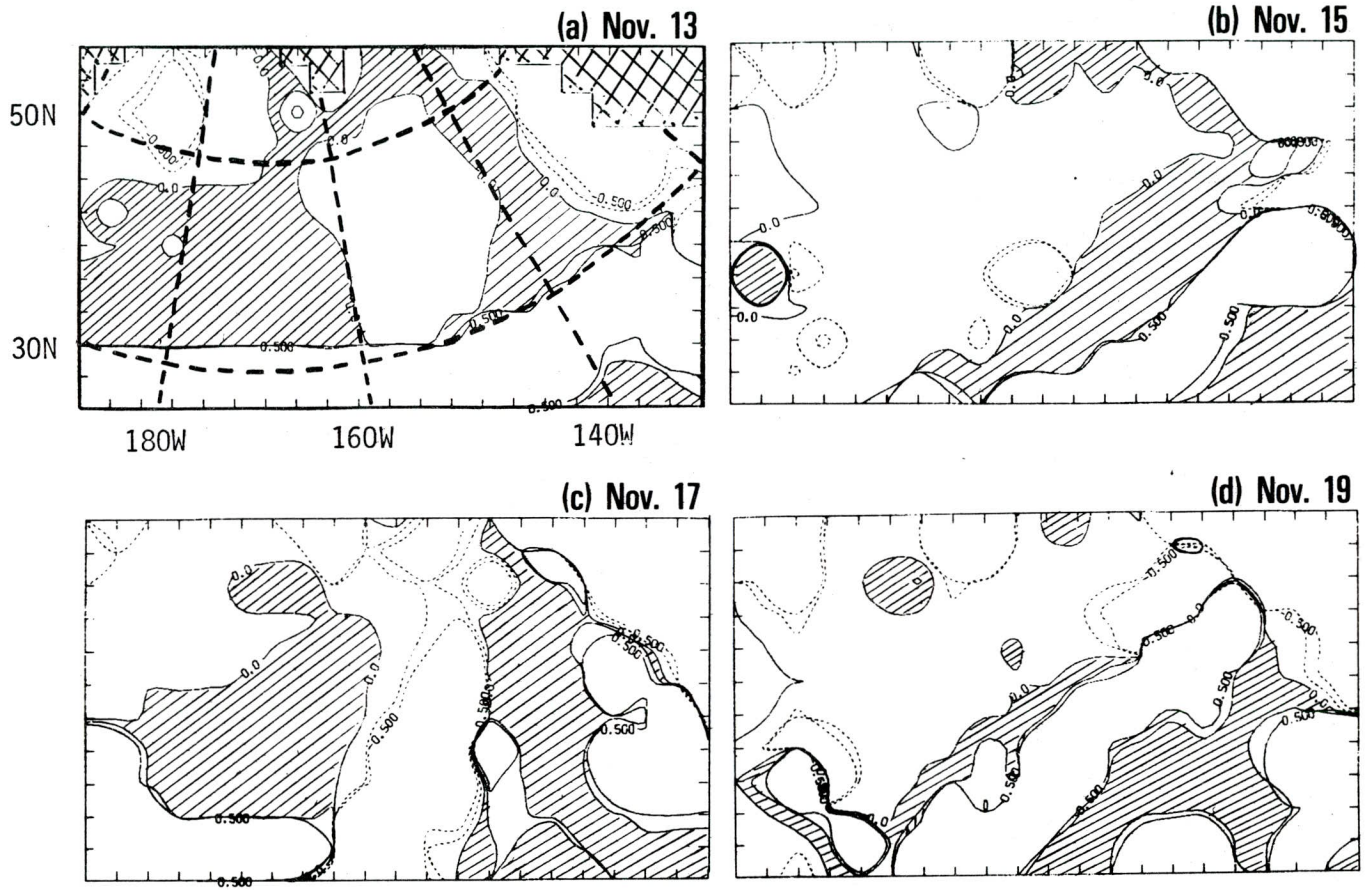

Figure 11. Synoptic variation of 10 m Ri in the North Pacific for 13-19 Nov 76.

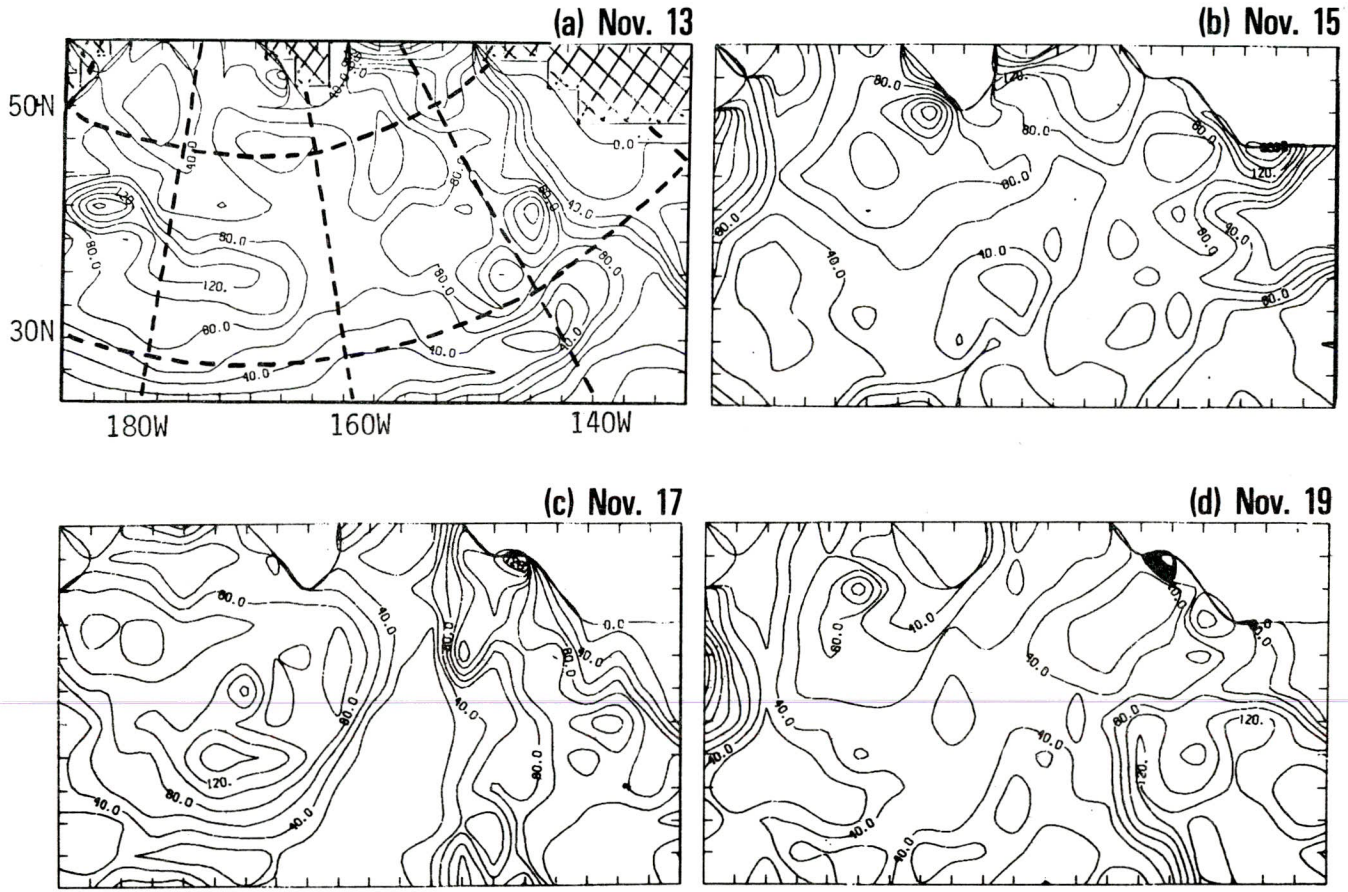

Figure 12. Synoptic variation of 7.5 m shear (s^{-1} x 10^4) in the North Pacific for 13-19 Nov 76.

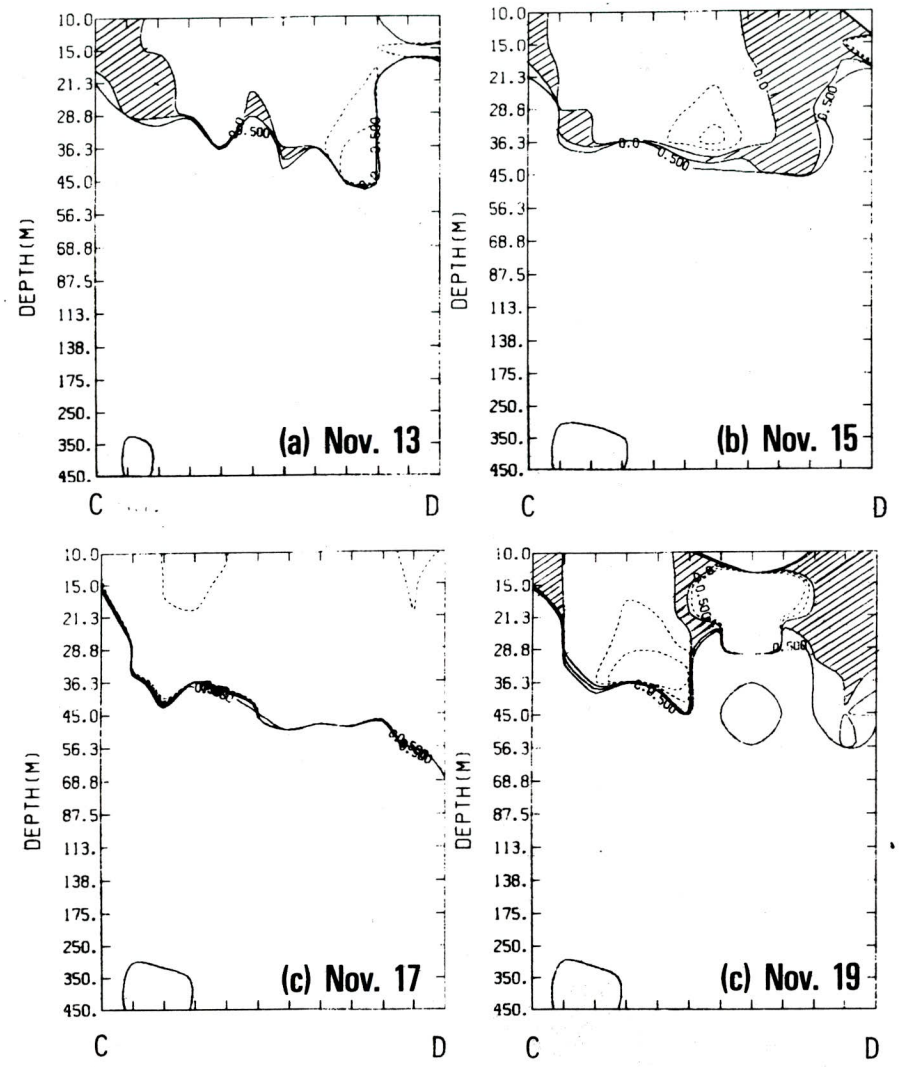

Figure 13. Synoptic variation of Ri along C-D cross-section for 13-19 Nov 76.

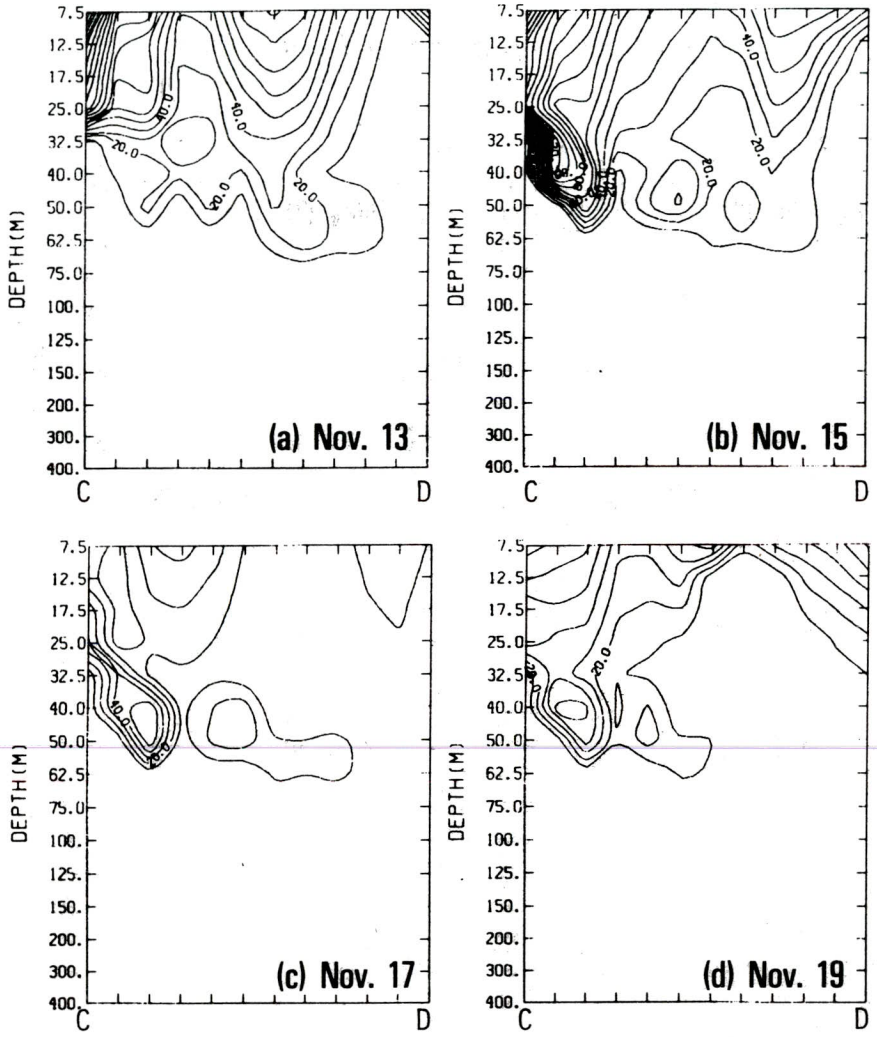

Figure 14. Synoptic variation of shear (s^{-1} x 10^4) along C-D cross-section for 13-19 Nov 76.

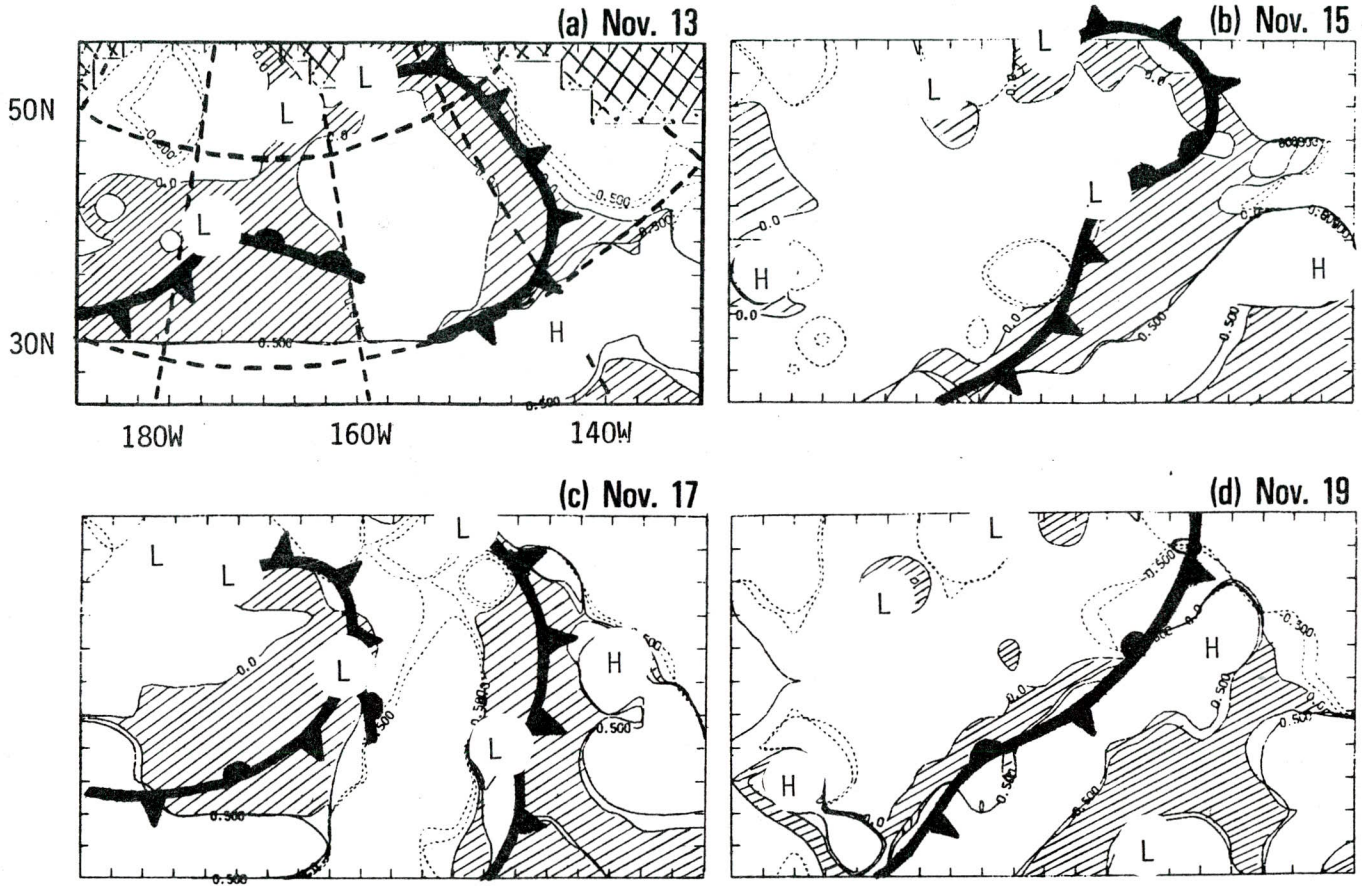

Figure 15. Superposition of synoptic weather patterns and 10 m Ri in the North Pacific for 13-19 Nov 76.

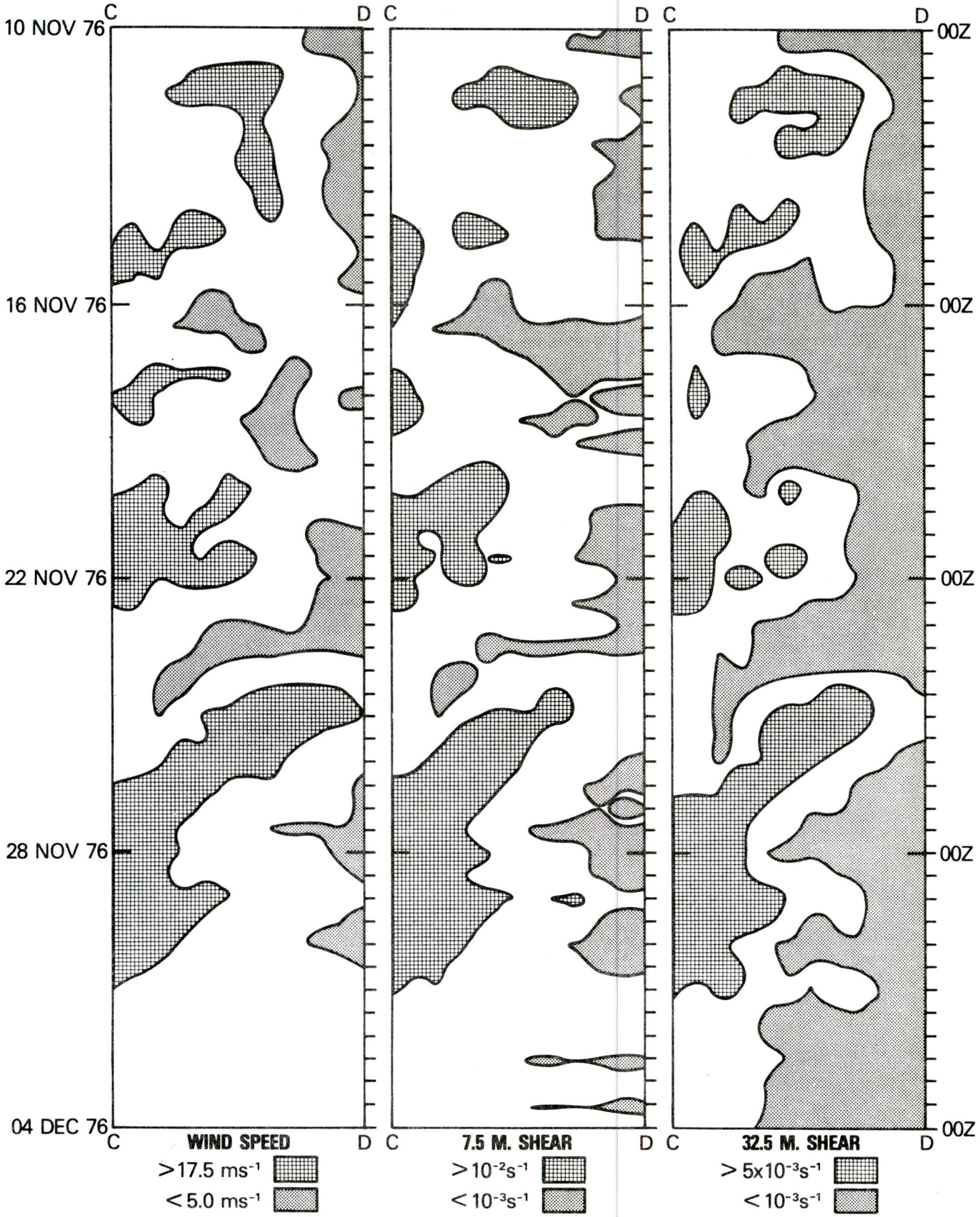

Figure 16. Phase plots of 12 hourly wind speed, 7.5 m and near pycnocline (32.5 m) shear in the North Pacific for 10 Nov 76 to 4 Dec 76.

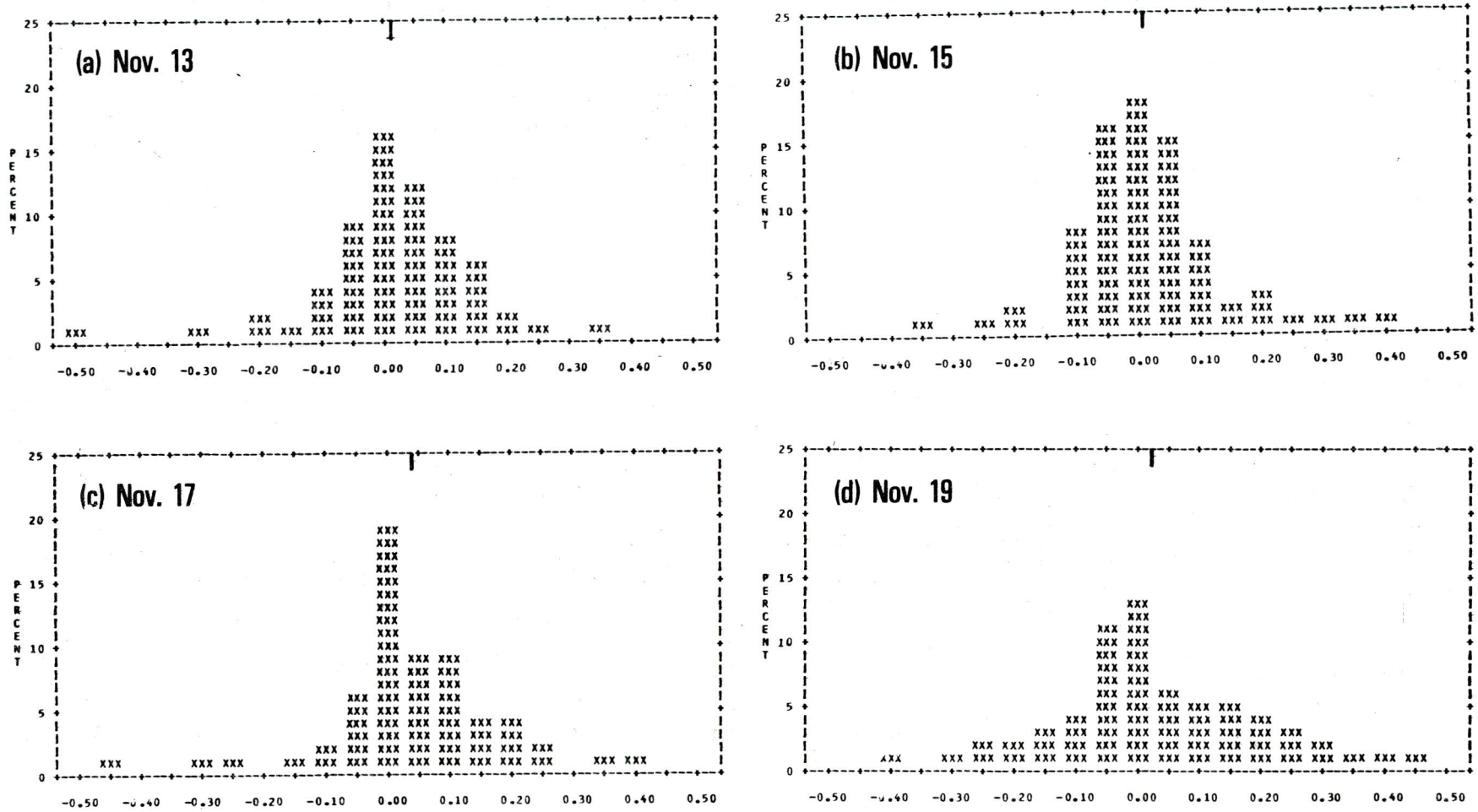

Figure 17. Frequency distribution of 10 m Ri in the North Pacific for 13-19 Nov 76.

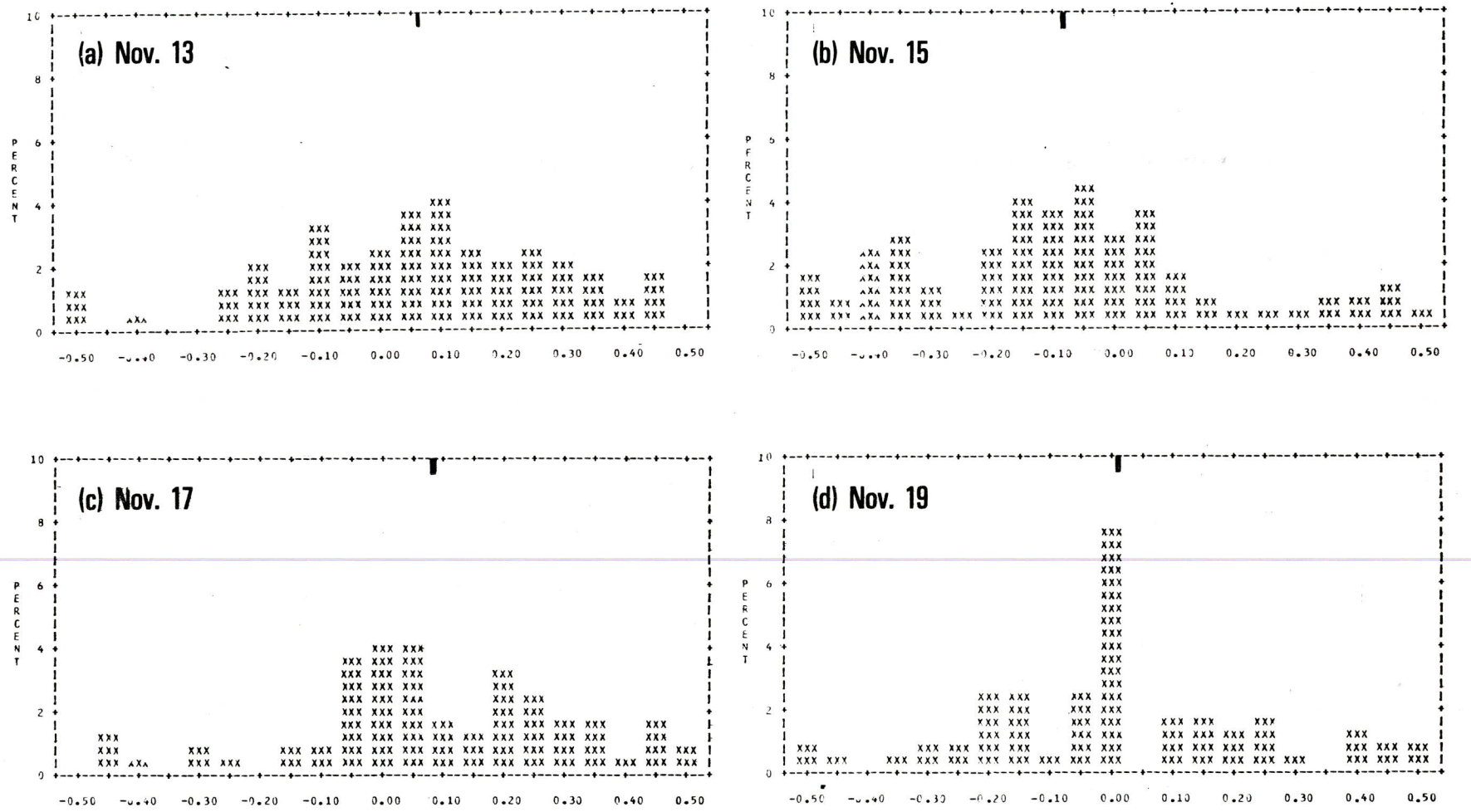

Figure 18. Frequency distribution of near pycnocline (36.3 m) Ri in the North Pacific for 13-19 Nov 76.

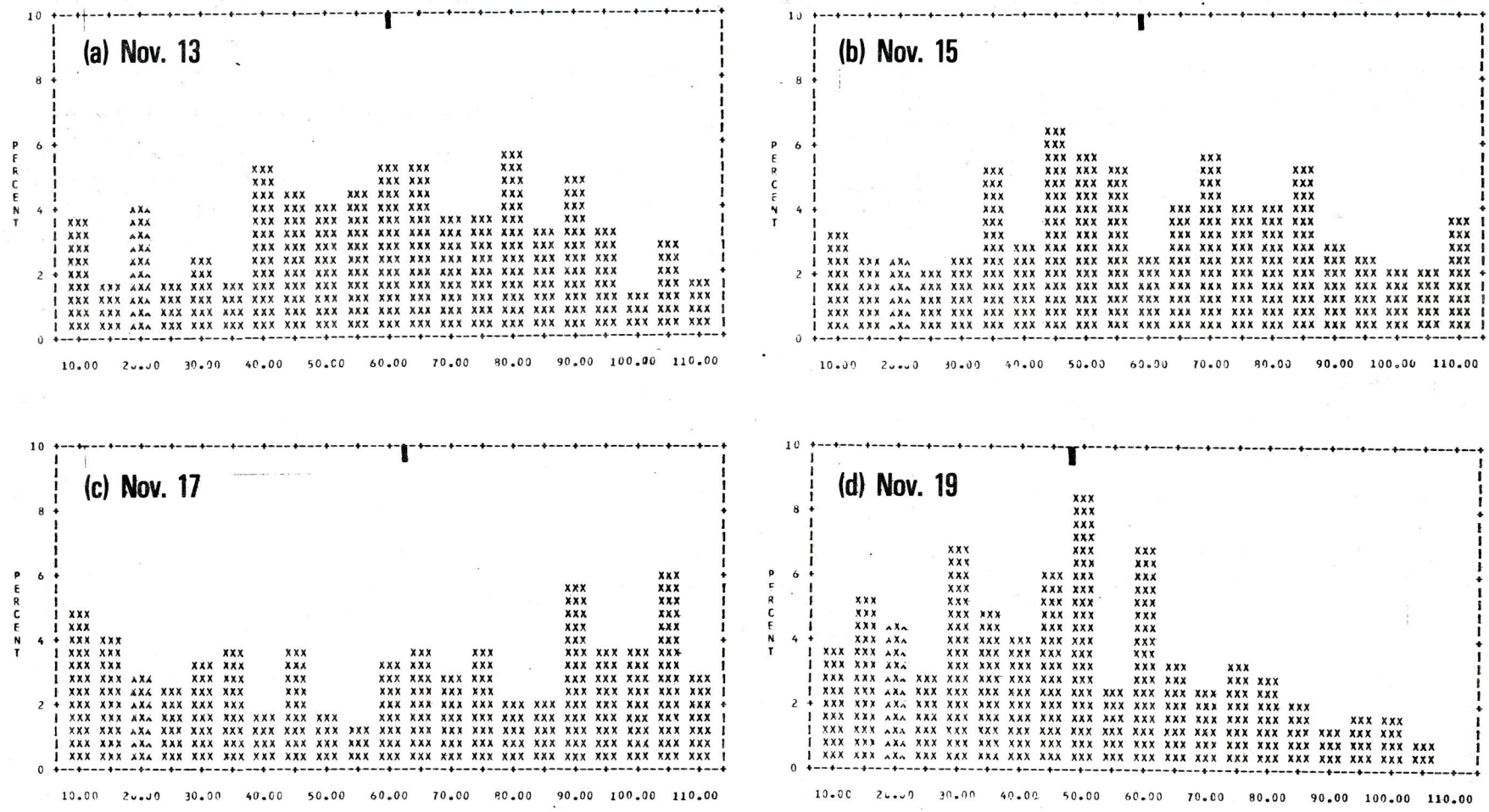

Figure 19. Frequency distribution of 7.5 m shear (s^{-1} x 10^4) in the North Pacific for 13-19 Nov 76.

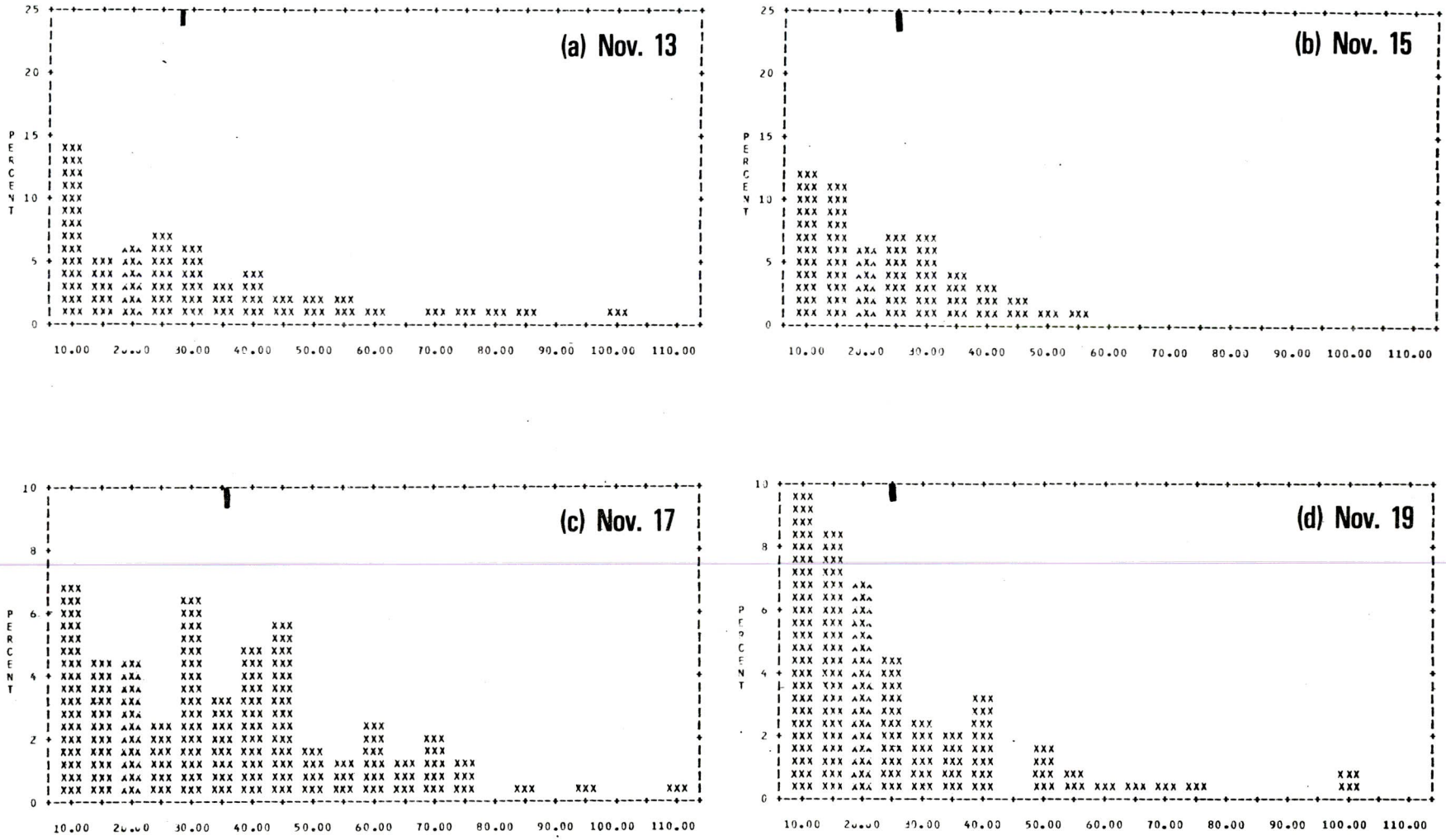

Figure 20. Frequency distribution of near pycnocline (32.5 m) shear (s^{-1} x 10^4) in the North Pacific for 13-19 Nov 76.

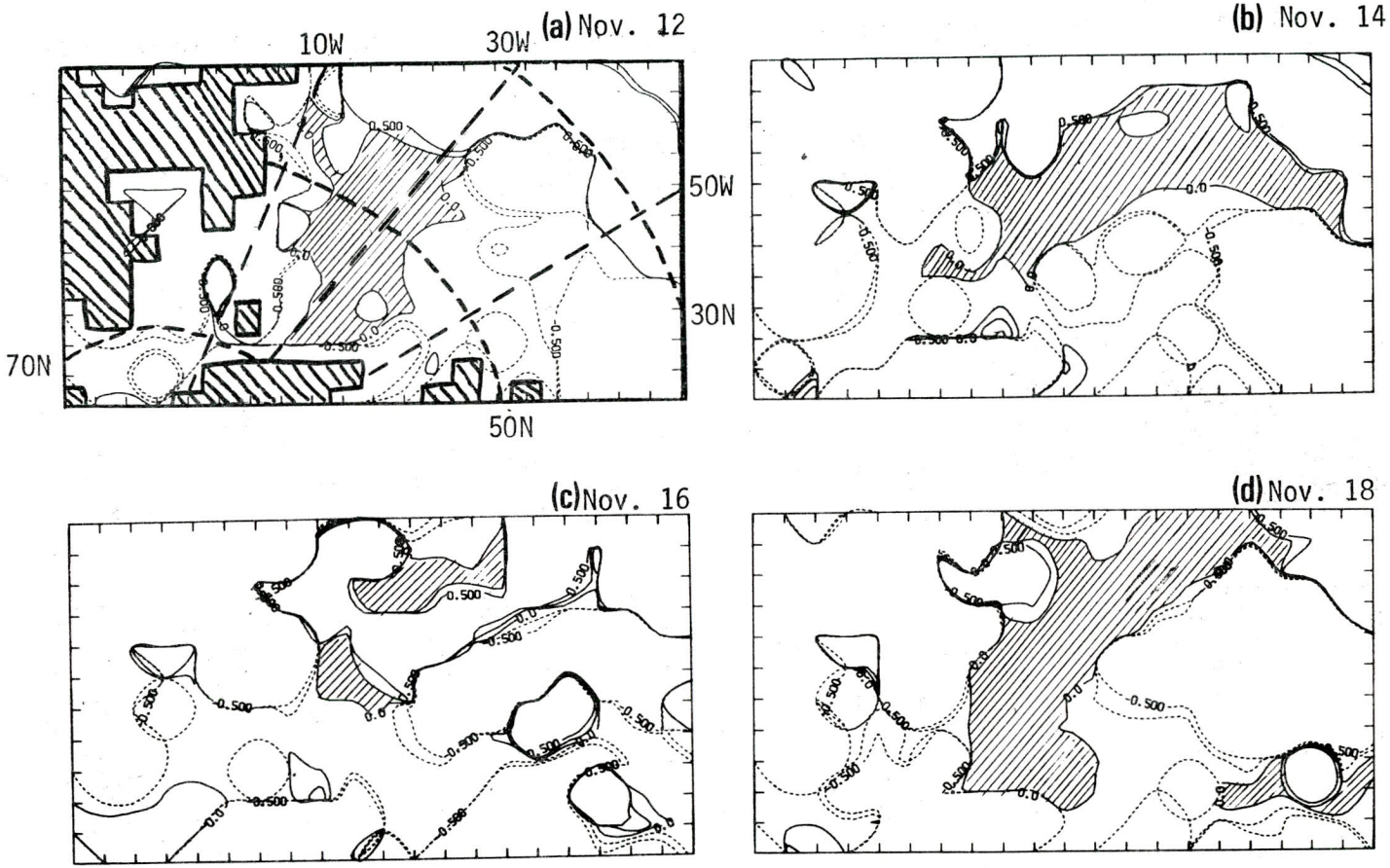

Figure 21. Synoptic variation of 10 m Ri in the North Atlantic for 12-18 Nov 76.

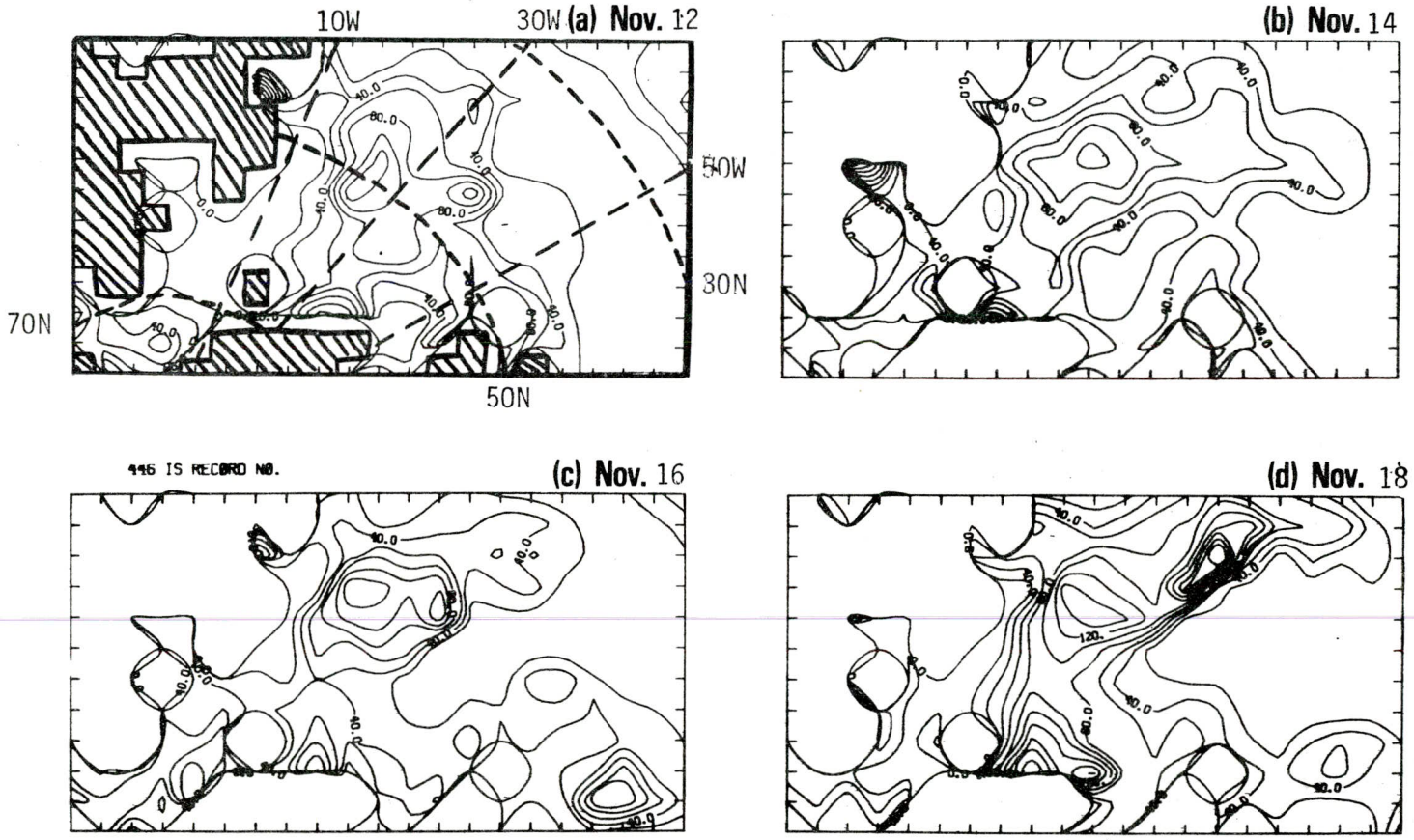

Figure 22. Synoptic variation of 7.5 m shear (s^{-1} x 10^4) in the North Atlantic for 12-18 Nov 76.

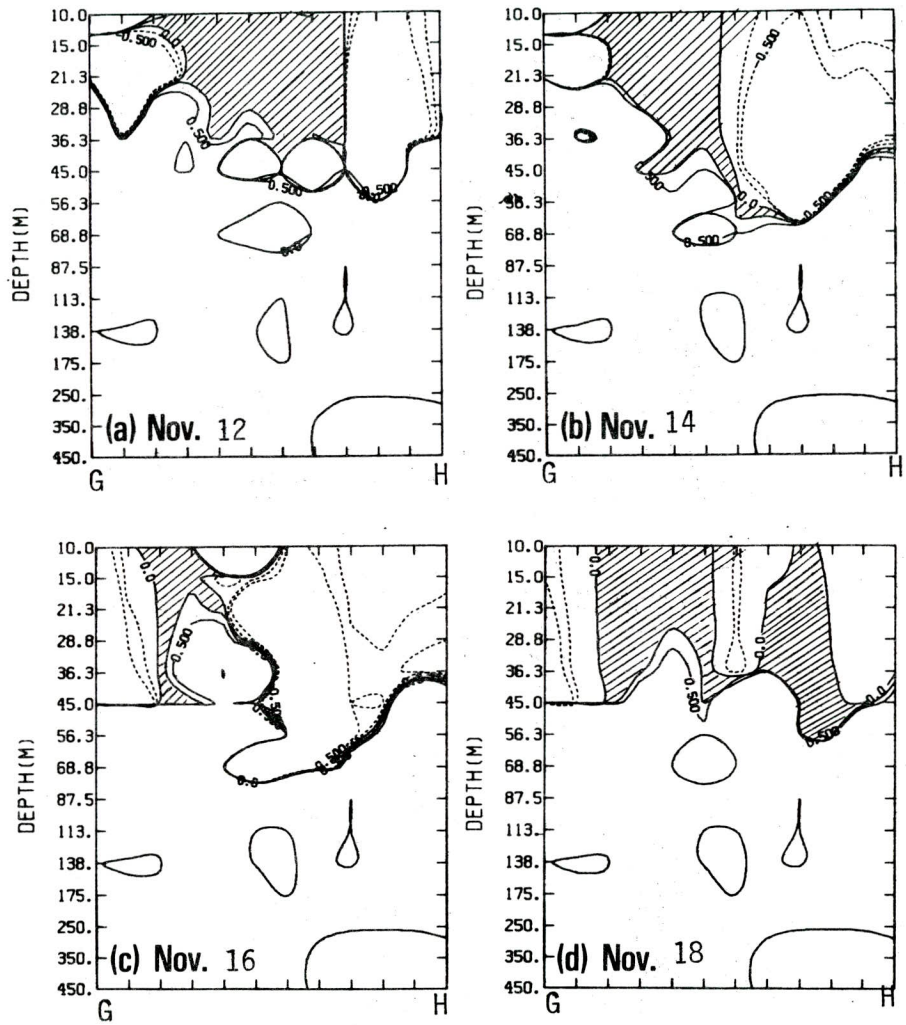

Figure 23. Synoptic variation of Ri along G-H cross-section for 12-18 Nov 76.

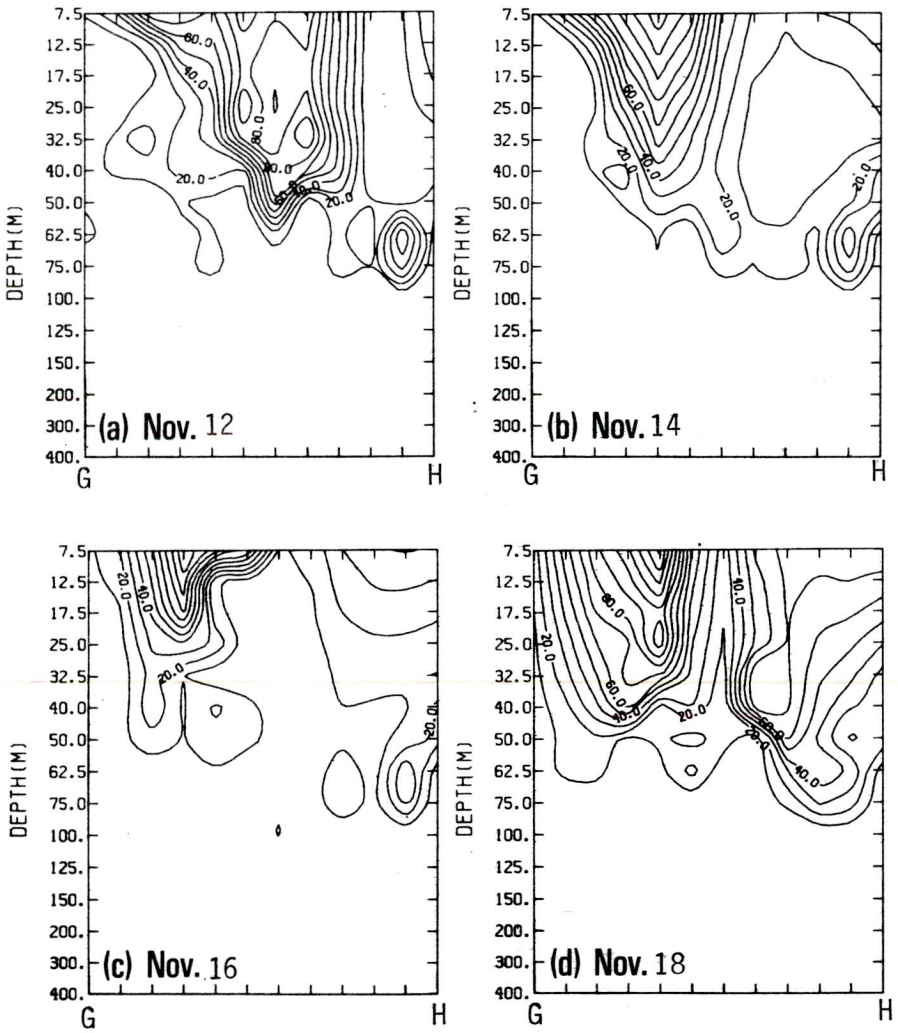

Figure 24. Synoptic variation of shear (s^{-1} x 10^4) along G-H cross-section for 12-18 Nov 76.

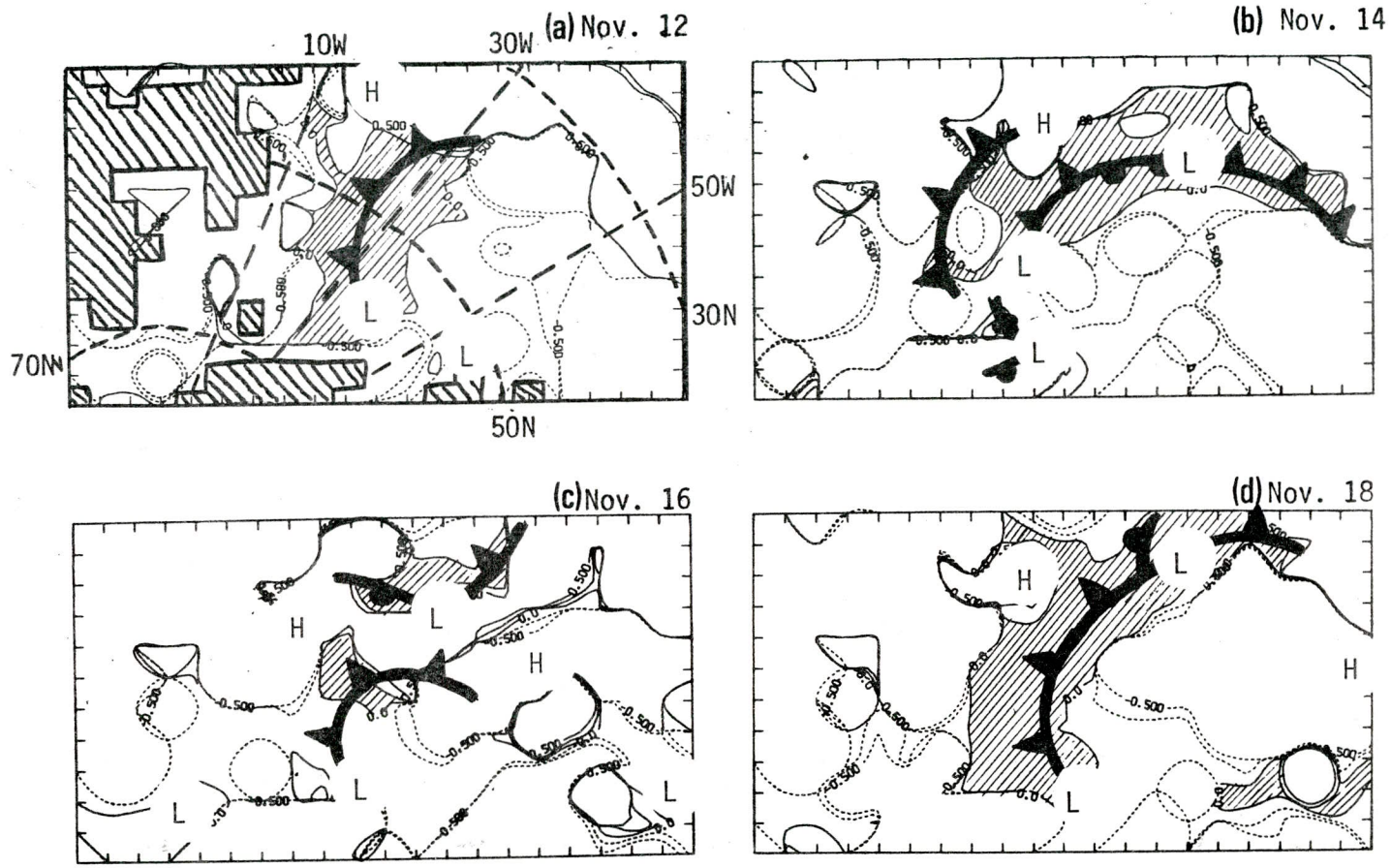

Figure 25. Superposition of synoptic weather patterns and 10 m Ri in the North Atlantic for 12-18 Nov 76.

SIGNIFICANT SHEAR - SYNOPTIC SCALE

		12 Nov (12L)	14 Nov (12L)	16 Nov (12L)	18 Nov (12L)
N. Pacific 76	Depth (m)				
% Shear $>10^{-3}$/s ,	7.5	87.5	93.5	85.3	88.8
	32.5	45.4	50.2	45.9	34.6
% Shear $>5 \times 10^{-3}$/s,	7.5	60.6	61.9	60.6	42.9
	32.5	8.2	5.6	10.4	3.5
N. Atlantic 76	Depth (m)				
% Shear $>10^{-3}$/s ,	7.5	57.2	75.4	70.3	71.8
	32.5	31.8	31.8	31.8	38.5
% Shear $>5 \times 10^{-3}$/s,	7.5	29.7	29.7	22.6	42.0
	32.5	7.1	5.7	4.1	11.3

Figure 26. Significant shear in the North Pacific and North Altantic for 12-18 Nov 76 (1200 local time).

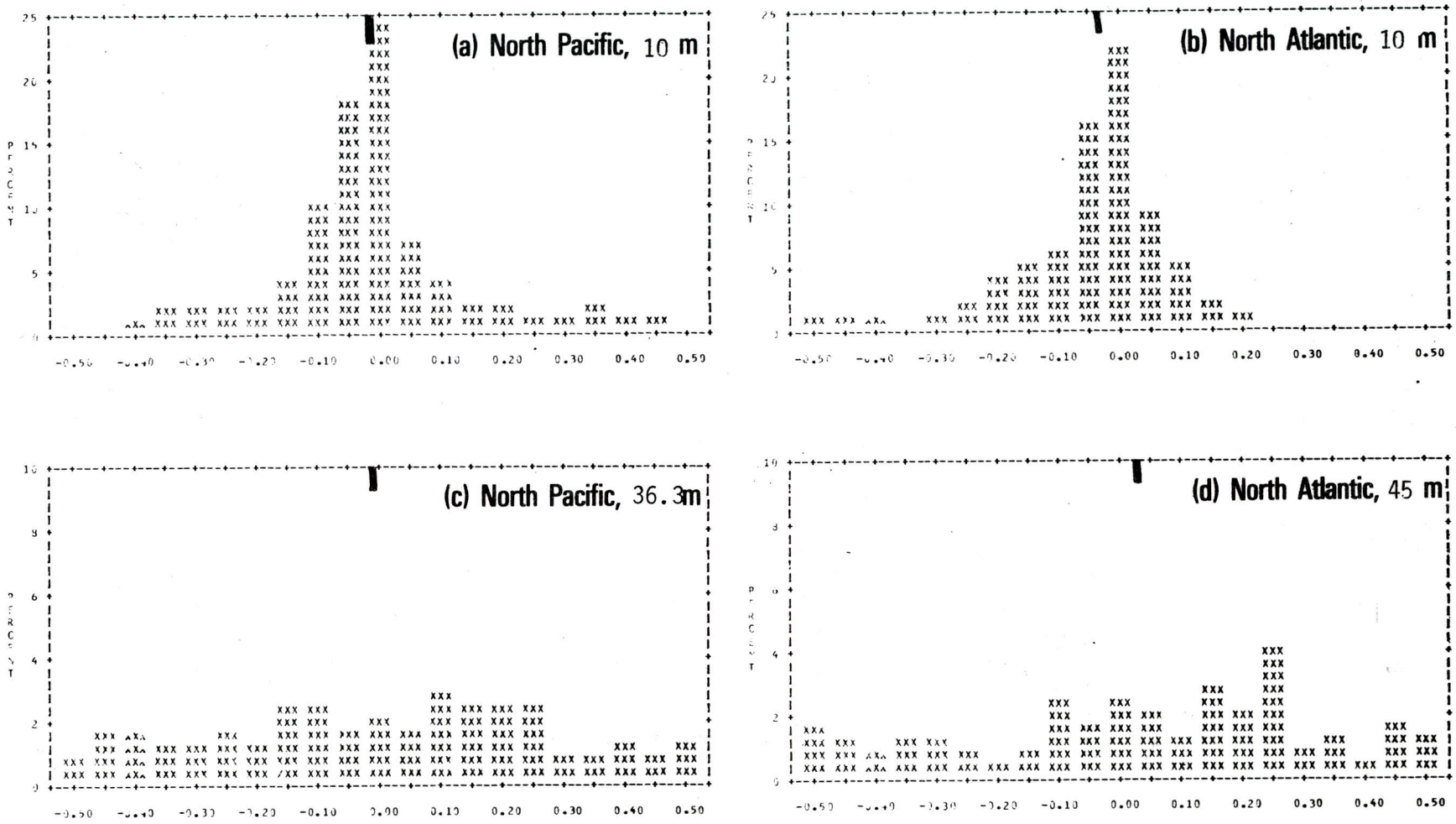

Figure 27. Cumulative frequency distribution of Ri at mid-domain grid points for Nov-Dec 1976 at 10 m in (a) the North Pacific and (b) North Atlantic and at near pycnocline depths in (c) the North Pacific and (d) North Atlantic.

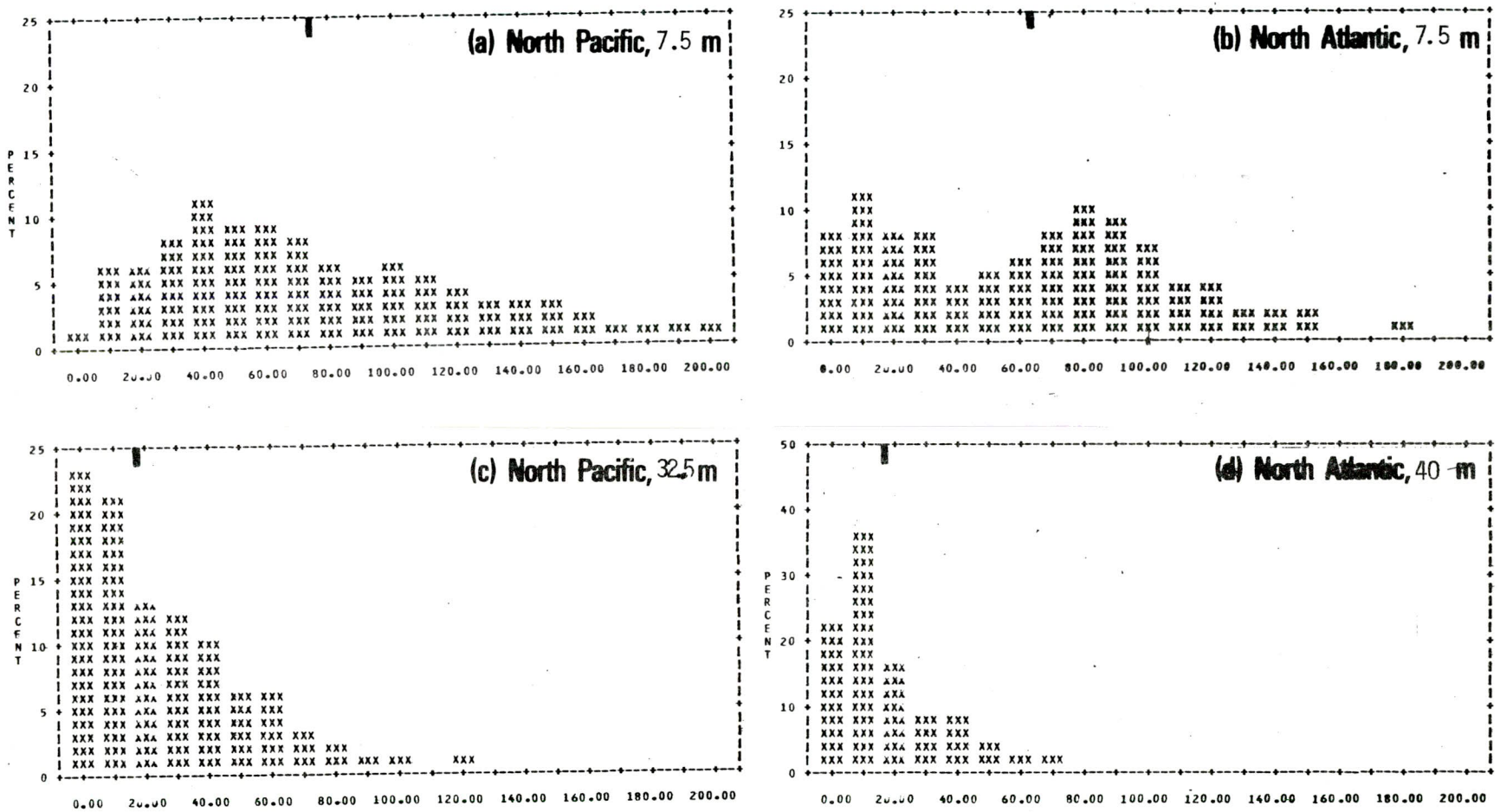

Figure 28. Cumulative frequency distribution of shear (s^{-1} x 10^4) at mid-domain grid points for Nov-Dec 1976 at 7.5 m in (a) the North Pacific and (b) North Atlantic and at near pycnocline depths in (c) the North Pacific and (d) North Atlantic.

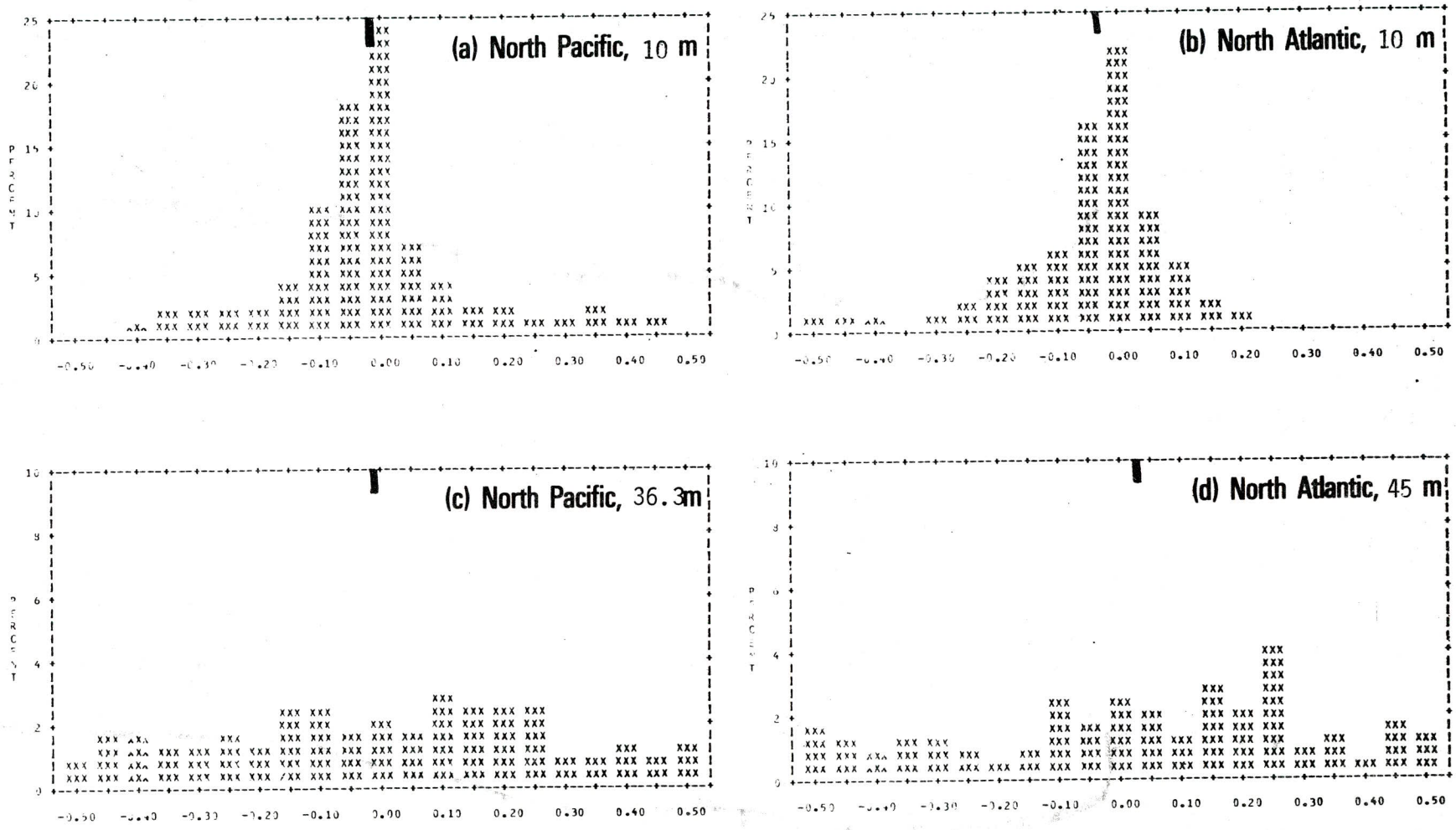

Figure 27. Cumulative frequency distribution of Ri at mid-domain grid points for Nov-Dec 1976 at 10 m in (a) the North Pacific and (b) North Atlantic and at near pycnocline depths in (c) the North Pacific and (d) North Atlantic.

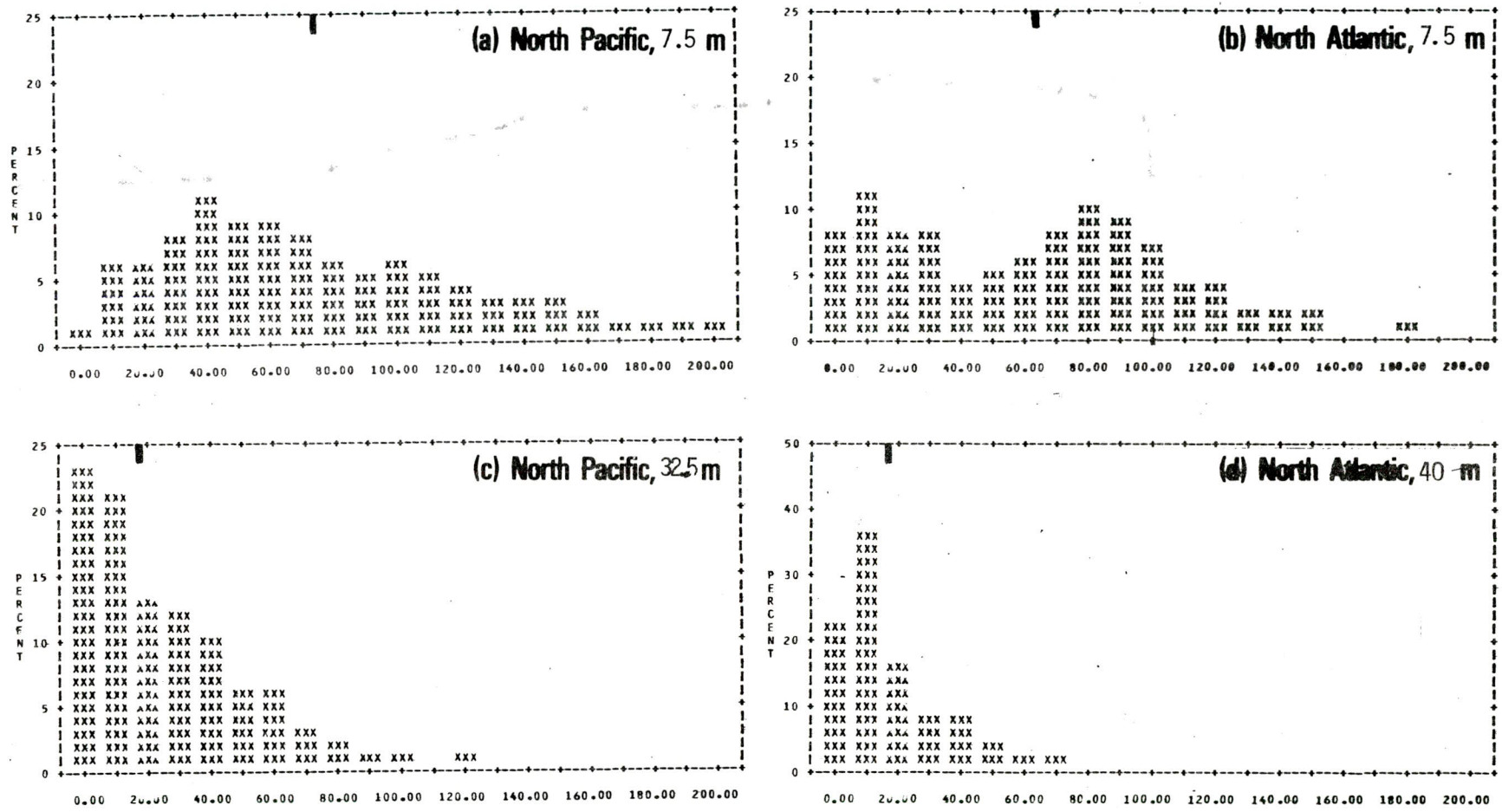

Figure 28. Cumulative frequency distribution of shear ($s^{-1} \times 10^{4}$) at mid-domain grid points for Nov-Dec 1976 at 7.5 m in (a) the North Pacific and (b) North Atlantic and at near pycnocline depths in (c) the North Pacific and (d) North Atlantic.

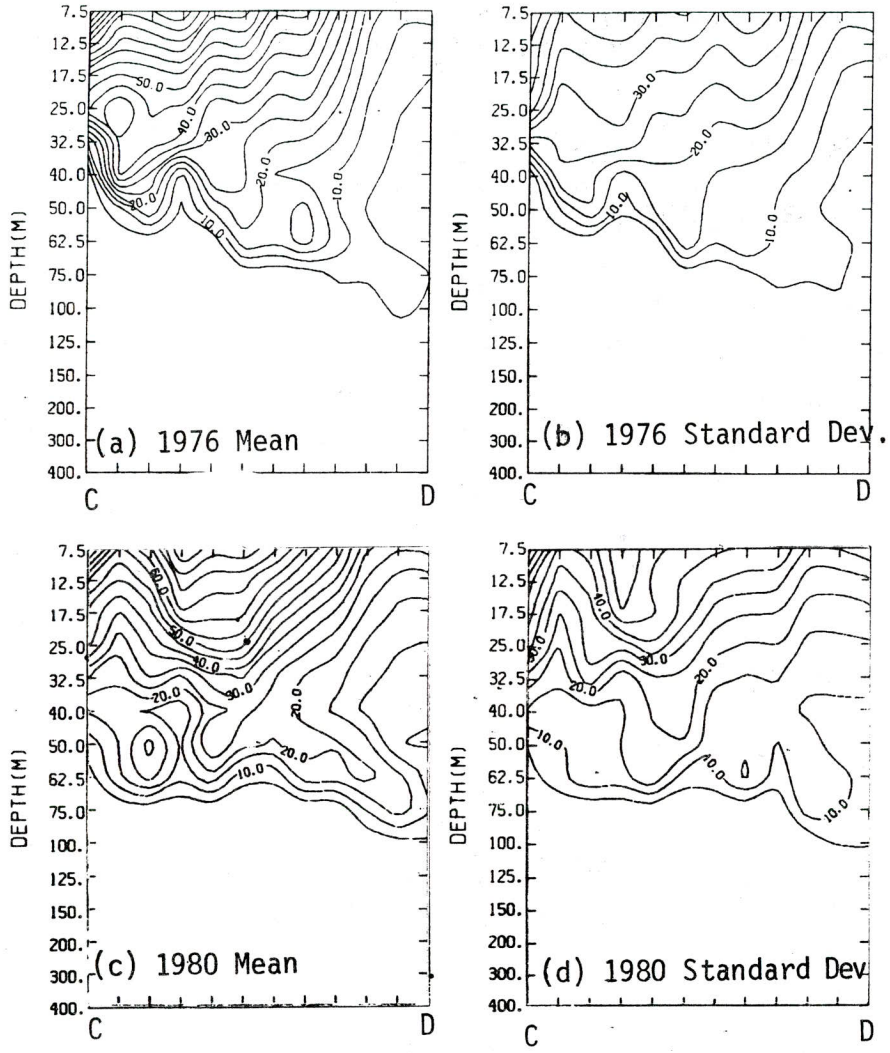

Figure 29. Interannual variation of shear (s^{-1} x 10^4) along C-D cross-section shown by Nov-Dec 1976 (a) mean and (b) standard deviation, compared with Nov-Dec 1980, (c) mean and (d) standard deviation.

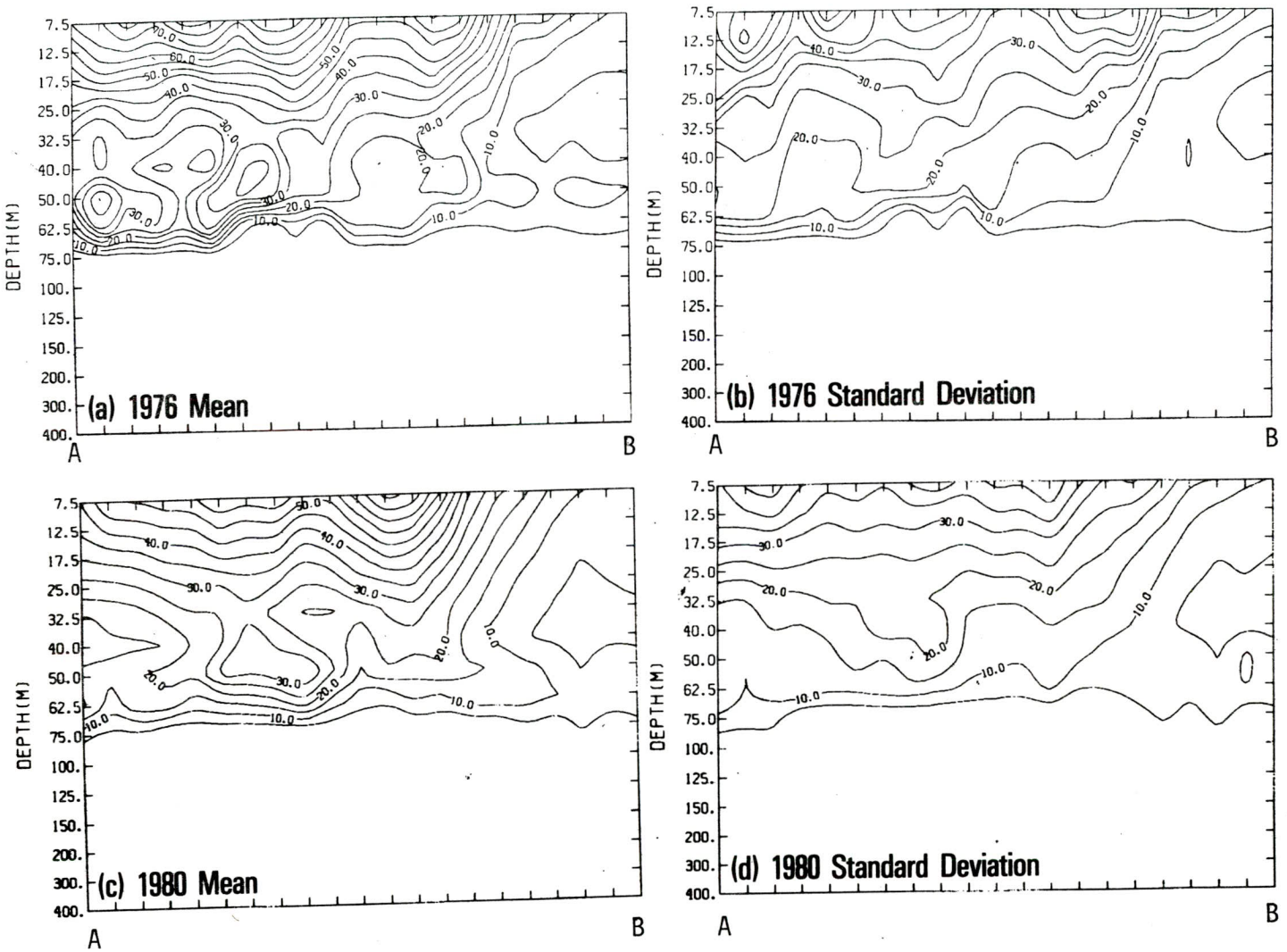

Figure 30. Interannual variation of shear (s^{-1} x 10^4) along A-B cross-section shown by Nov-Dec 1976 (a) mean and (b) standard deviation, compared with Nov-Dec 1980, (c) mean and (d) standard deviation.

UNCLASSIFIED

SECURITY CLASSIFICATION OF THIS PAGE *(When Data Entered)*

REPORT DOCUMENTATION PAGE		READ INSTRUCTIONS BEFORE COMPLETING FORM
1. REPORT NUMBER NORDA Technical Note 206	2. GOVT ACCESSION NO.	3. RECIPIENT'S CATALOG NUMBER
4. TITLE *(and Subtitle)* Statistics of Vertical Shear from a Hemispheric Model		5. TYPE OF REPORT & PERIOD COVERED Final
		6. PERFORMING ORG. REPORT NUMBER
7. AUTHOR*(s)* J. M. Harding R. H. Preller S. A. Piacsek		8. CONTRACT OR GRANT NUMBER*(s)*
9. PERFORMING ORGANIZATION NAME AND ADDRESS Naval Ocean Research & Development Activity Ocean Science and Technology Laboratories NSTL, Mississippi 39529		10. PROGRAM ELEMENT, PROJECT, TASK AREA & WORK UNIT NUMBERS 63704N
11. CONTROLLING OFFICE NAME AND ADDRESS Same		12. REPORT DATE September 1983
		13. NUMBER OF PAGES 46
14. MONITORING AGENCY NAME & ADDRESS*(if different from Controlling Office)*		15. SECURITY CLASS. *(of this report)* UNCLASSIFIED
		15a. DECLASSIFICATION/DOWNGRADING SCHEDULE

16. DISTRIBUTION STATEMENT *(of this Report)*

Approved for Public Release
Distribution Unlimited

17. DISTRIBUTION STATEMENT *(of the abstract entered in Block 20, if different from Report)*

18. SUPPLEMENTARY NOTES

19. KEY WORDS *(Continue on reverse side if necessary and identify by block number)*

ocean shear prediction
oceanic shear forecasting
oceanic shear
vertical shear
inertial shear
Ekman shear
TOPS

20. ABSTRACT *(Continue on reverse side if necessary and identify by block number)*

Using surface atmospheric momentum and heat fluxes derived from the Fleet Numerical Oceanography Center's weather prediction models, a computation of inertial and Ekman shear was done for the upper 400 m of the North Pacific and North Atlantic. Two 60-day periods were considered in November and December of 1976 and 1980. A capability to predict these types of shear in real-time, or near real-time, is demonstrated using the Navy's TOPS (Thermodynamic Ocean Prediction System) model. A statistical analysis of the vertical shear and

DD FORM 1 JAN 73 1473 EDITION OF 1 NOV 65 IS OBSOLETE
S/N 0102-LF-014-6601

UNCLASSIFIED

SECURITY CLASSIFICATION OF THIS PAGE *(When Data Entered)*

associated Richardson number revealed that the time variability of shear appears to be linked primarily to the synoptic time scales of weather events; and the spatial distribution of shear instability ($0 \leq Ri \leq 0.25$) and high shear are closely related to the position of atmospheric fronts.